

# Spectroscopy of Dwarf HII Galaxies in the Virgo Cluster. I. Data, Chemical Abundances and Ionization Structure

José M. Vílchez

jvm@iaa.es

*Instituto de Astrofísica de Andalucía (CSIC)*

*Apdo. 3004, 18080 Granada, SPAIN*

and

Jorge Iglesias-Páramo

jorge@astrsp-mrs.fr

*Laboratoire d'Astrophysique de Marseille*

*Traverse du Siphon, F-13376, Marseille Cedex 12, FRANCE*

## ABSTRACT

Long-slit spectroscopy has been obtained for a sample of 22 blue dwarf galaxies selected in the direction of the Virgo Cluster as part of a larger sample of Virgo blue dwarf galaxies for which deep H $\alpha$  imaging has been collected. Most of the galaxies in the present sample appear classified as BCDs or dwarf Irregulars in the Virgo Cluster Catalog. Line fluxes, H $\beta$  equivalent width and extinction coefficients, spatial emission profiles, ionization structure and physical conditions are presented for the galaxies of the sample. Chemical abundances have been derived either using a direct determination of the electron temperature or after detailed examination of the predictions of different empirical calibrations. The oxygen abundance derived for the sample of Virgo dwarf galaxies span in the range  $7.6 \leq 12 + \log \text{O}/\text{H} \leq 8.9$ , and the corresponding nitrogen to oxygen abundance ratio cover from values typical of low metallicity field BCD galaxies up to near solar.

*Subject headings:* galaxies: abundances — galaxies: ISM: HII regions — galaxies: dwarf — galaxies: clusters: individual (Virgo)

## 1. Introduction

Within the study of the evolution of galaxies it appears now well established that the environment is playing a significant role. From theoretical grounds, it could be expected that galaxies located in high density regions such as clusters of galaxies may suffer the effects of interactions, giving rise to a certain degree of mass losses or mass redistribution. Also, after the interaction with the (hot) intracluster medium (ICM), the gaseous component of galaxies may be affected by ram pressure stripping or evaporation (Haynes et al. 1984). The relatively high density of the ICM together with the higher probability of encounters in (rich) clusters may produce selective losses of gaseous galactic material. In this respect, the existence of a morphology-density relation is in the line of the observed deficit of gas-rich dwarf galaxies in dense environments (*e.g.* Binggeli et al. 1987).

A direct environmental impact is expected to be observed in the activity of star formation in galaxies (*e.g.* Hashimoto et al. 1998; Iglesias-Páramo & Vílchez 1999). This fact is of particular relevance for the issue of galaxy evolution, owing to the strong implications that gas flows (in/outflows), as well as gas stripping and/or pressure confinement, may have for the study of the chemical evolution of galaxies. The observational results available show a significant difference in the observable HI content between cluster and field spirals, the Virgo ones being HI deficient (*e.g.* Cayatte et al. 1990; Solanes et al. 2001). Other results obtained for the molecular component however, show that the cold molecular clouds located near the center of these galaxies, which accumulate large amounts of H<sub>2</sub> and CO, do not appear to disintegrate into the ICM (Kenney & Young, 1988; Boselli et al. 1997). Since gas-rich dwarf galaxies are fragile systems, because they show low mass surface densities and rotation velocities (Gallagher & Hunter 1989; 1984), it is expected that the impact of the environment should be significant for these objects. However, Hoffman et al. (1988) studied a large sample of dwarf galaxies in Virgo and found that, on average, they were not more stripped than spirals. The sole existence of these HI -rich dwarf galaxies in such a hostile environment pose serious questions to be investigated further.

Analysis of the spectroscopic properties of local and distant samples of emission-line galaxies belonging to environments of different density, show that galaxies in higher density regions may appear statistically associated to somewhat lower star formation rates (Hashimoto et al. 1998; Vílchez, 1995). Similar studies of emission line galaxies located in or near voids, specially at lowest density, point to levels of star formation activity comparable to, or slightly higher than field galaxies (*cf.* Popescu et al. 1999; Grogin and Geller 2000). At this point, the question has arisen as to whether other fundamental properties of dwarf galaxies, such as their metal content, may feel the impact of their environment. It has been claimed that this can be the case of the so called tidal dwarf galaxies (Duc and

Mirabel 1999; Vílchez 1999); nonetheless, the study of the global spectroscopic properties of a sample of star-forming dwarfs in different environments (Vílchez 1995) led to the conclusion that the majority of them follow rather well a metallicity-luminosity relation. Some of the Virgo dwarfs studied in the latter work presented distinct spectroscopic properties and it was suggested they may hold a larger abundance though no definitive conclusion could be reached until more and better data are available. In the present work new and better spectroscopic data have been collected for a sample of Virgo dwarfs. A subsequent investigation has been undertaken in order to study their chemical evolution, and the impact of environmental effects. Their relative contribution to the metal enrichment of the ICM and to the overall metallicity-(mass)-luminosity relation will be presented in a forthcoming paper (Vílchez et al. 2002 in preparation; paper II).

Several Virgo dwarf galaxies have been already studied spectroscopically (Gallagher & Hunter 1989; Izotov & Guseva, 1989; Lee et al. 2000) or multirange (*e.g.* Brosch et al. 1998). The present work is aimed to produce a systematic spectroscopic study of a large sample of star-forming dwarf galaxies in the Virgo Cluster. Previous results for dIrr in Virgo (*e.g.* IC 3475, Vigroux et al. 1986; UGC 7636, Lee et al. 2000) and, more recently in A 1367 (CGCG 97-073 and CGCG 97-079, Gavazzi et al. 2001, Iglesias-Páramo et al. 2002) have shown direct evidences that ram pressure stripping is at work for cluster dwarf galaxies.

Finally, the location of our sample dwarfs in the Virgo cluster would allow the star forming regions to be spatially resolved and, since all share approximately the same distance, minimizing all the distance-dependent uncertainties in the analysis. In section 2 of this paper we report on the observations and data obtained for the sample galaxies. In section 3, the results derived for the ionization structure, physical properties and chemical abundances are presented. The discussion and conclusions from the analysis of the results are presented in section 4. Further work including the implications of these results for the spectrophotometric evolution of the Virgo dwarf galaxy sample and a global discussion of their properties will be presented in paper II.

## 2. Observations and Data Reduction

Within an ongoing project of deep imaging of the BCD and Irregular galaxies in the Virgo Cluster Catalog (VCC; Binggelli et al. 1985), a total sample of 22 objects (21 Virgo plus 1 background) most of them classified as blue compact dwarf galaxies, were selected for our spectroscopic study. All the galaxies were selected in the direction of the Virgo central field (sampling within a radius  $\sim 5$  degrees from M 87) for which our H $\alpha$  survey is being carried out (Boselli et al. 2002). The majority of the objects in the sample belong to VCC

morphological classes BCD, Im/BCD; some of them appear classified as Im, Sm, and few other are quoted peculiar Sp/BCD, dS<sup>?</sup>/BCD<sup>?</sup> or amorphous (*cf.* Gallagher and Hunter 1989).

The observations were carried out at the Observatorio del Roque de los Muchachos (ORM, La Palma) during two three-nights runs, using the 4.2-m William Herschel Telescope (WHT) with the ISIS double-arm spectrograph at the Cassegrain focus. For each slit position two spectra, one in the red and one in the blue, were taken simultaneously using the corresponding dichroic. Typical seeing values were around 0."8 to 1" throughout the runs, oscillating around 2" during the second part of the 1994 run. During the first part of the 1993 run light high cirrus were present. All the exposures during both runs were made as closer to the zenith as possible (airmasses were always  $\leq 1.3$  except in one case, VCC 428, observed at 1.5) in order to minimize any differential atmospheric refraction effects.

The 1280 $\times$ 1180 EEV3 detector with 22.5- $\mu$ m pixels was used for the red arm, and a 1124 $\times$ 1124 TEK1 with 24- $\mu$  pixels for the blue arm. The effectively observed detector area was windowed to 1230 and 1020 pixels in the spectral direction for the EEV3 and TEK1 detectors, respectively, and to 600 pixels along the slit for both detectors. The spatial scale was of 0.335 " pixel<sup>-1</sup> and 0.357 " pixel<sup>-1</sup> for the EEV3 and TEK1 detectors, respectively, giving a total slit length of approximately 3.4 '.

The dichroic was set at an effective wavelength of  $\lambda$  5400 Å (1993) and  $\lambda$  5700 Å (1994) in order to separate the spectral ranges of the blue and red arms. The 316R grating used for the red arm had 316 line mm<sup>-1</sup> yielding a reciprocal dispersion of 60.4 Å mm<sup>-1</sup>. The 300B grating used for the blue arm had 300 line mm<sup>-1</sup> yielding a reciprocal dispersion of 62.2 Å mm<sup>-1</sup>. A similar effective spectral resolution of 4 Å FWHM was reached for both arms.

An additional spectral range in the near infrared was observed for two of the galaxies, VCC 1699 and VCC 144, centered at  $\lambda$  9100 Å. This observational set up allowed us a total spectral coverage which includes lines from [O II]  $\lambda$  3727 Å up to [S III]  $\lambda$  9520 Å.

The journal of observations is shown in Table 1. For each galaxy the VCC number (Column 1), other name (column 2), morphological type <sup>1</sup> (column 3), 1950 coordinates (columns 4, 5), slit position angle (column 6), central wavelength (column 7), total exposure (column 8) and date of the observation (column 9) are presented.

The data reduction was performed at the IAC using the standard software package

---

<sup>1</sup>For a definition of the morphological types see Binggeli, Sandage & Tamman (1985); Sandage (1961), Sandage & Tamman (1981), Sandage & Binggeli (1984)

IRAF<sup>2</sup>, following the standard procedure of bias correction, flatfielding, wavelength calibration, sky subtraction and flux calibration. The correction for atmospheric extinction was performed using an average curve for the continuous atmospheric extinction at the ORM (King 1985); flux calibration was achieved using repeated observations of the standards sp1446+259 and sp0642+021 from the La Palma spectrophotometric set (Sinclair, 1996) which were observed throughout both runs. The sky subtraction process was efficient for most of the spectra, though the proximity of the Na I D feature (sky and Galactic) to the emission of He I  $\lambda$  5876 Å in some spectra might contaminate the flux measured for this line.

Figure 1 show the spatial profiles of the galaxies (line plus continuum flux) along the slit position, extracted from the 2-D spectra at the wavelength corresponding to the H $\alpha$  line for each galaxy. Many of the spatial profiles are consistent with a single central source of emission, though some galaxies present a rich spatial structure. This is the case of VCC 848 for which up to four emission peaks can be disentangled in the spatial profile. Three spectra were extracted, labeled (a), (b) and (c) in Figure 1 –given the low signal to noise (S/N) of the emission lines in the fourth peak–, in addition to the integrated spectrum.

In this work an integrated spectrum has been analyzed for each galaxy, extracted adding the flux in the set of spatial increments under the corresponding H $\alpha$  and H $\beta$  spatial profiles, in order to maximize the final S/N ratio. Representative spectra of all the galaxies of the sample are shown in Figure 2.

### 3. Results

#### 3.1. Line Intensities

Line intensities were measured using the task SPLOT running on the IRAF environment, by marking to continuum points around each line to be measured and adding the total excess flux over the continuum level within the two points. Errors were determined for each line by taking into account the poissonian error associated with the total number of counts in the line plus its continuum, the dispersion (rms) of the nearby continuum, the effect of background subtraction, as well as the error associated with the exact placement of the local continuum. Independent measurements of the spectra were carried out in order to produce final error estimates. We believe that, though the relative sources of error are of varying importance for each line, absolute errors in the flux of faint lines should be dominated by the

---

<sup>2</sup>Image Reduction and Analysis Facility, written and supported at the National Optical Astronomy Observatories

continuum subtraction. We have not given a formal error for the absolute flux calibration of the spectra; we estimate an average error to be in the range 15–20%.

Each arm of the spectrograph was independently flux calibrated; and the matching of the corresponding extremes of the blue and red spectra was fairly good, except in the case of VCC 848 (1993 run) and VCC 1437, for which the flux match between the spectra of both arms was rather poor and they were rescaled. The spectra of the galaxy VCC 848, which was independently observed (at slightly different positions) during the two runs, give results consistent within the errors.

In order to minimize the error associated with the relative (to  $H\beta$ ) flux calibration over the full wavelength range (especially for faint lines), whenever possible line ratios were derived with respect to the flux of the nearest Balmer line —  $H\beta$  or  $H\alpha$  —.

In Figure 2 all the spectra of the sample galaxies are shown. As illustrated in the Figure, the spectra do not fit into an homogeneous class. They cover a wide range in spectral properties, such as the equivalent width of the emission lines, the strength and shape of the underlying stellar continua as well as the strength of the Balmer lines in absorption and/or emission. As two illustrative examples of spectra of our sample we underline VCC 428, which shows the typical spectrum of an HII region with a very faint continuum and strong emission lines, and VCC 1179, which shows strong apparent absorption in the Balmer series and very faint emission lines.

Underlying Balmer absorption is clearly present in the spectra of many galaxies of the sample. In order to correct line fluxes from this effect, a selfconsistent procedure has been applied which performed a fit to the Balmer decrement taking into account the contributions of the extinction and the underlying absorption. In this procedure the equivalent width in absorption was assumed to be the same for all the Balmer lines used (from  $H\delta$  to  $H\alpha$ ), as expected for young ionizing clusters. The correction for underlying absorption applied ranges from equivalent widths equal to zero (*e.g.* for VCC 1313, VCC 802) up to values around 9 Å in some objects showing a strong continuum contribution (*e.g.* VCC 1179, VCC 135, VCC 1437). This range of values of the  $H\beta$  equivalent width in absorption were found to be enough to bring the observed Balmer ratios into the theoretical values, within the errors. All the spectra were corrected for reddening using the value of the Balmer decrement. The reddening coefficient,  $C(H\beta)$ , was derived using the ratios of the optical Balmer recombination lines once corrected from underlying absorption, compared to the theoretical values for case B recombination ( $H\alpha/H\beta = 2.85$ ,  $H\gamma/H\beta = 0.469$  and  $H\delta/H\beta = 0.260$ , Hummer & Storey 1987), and taking into account their S/N ratio and appropriate baseline corrections. The values derived for  $C(H\beta)$  vary from 0 to 0.5; and a typical error for the reddening coefficient is estimated to be around  $\pm 0.1$ .

Measurements of the flux in the  $[\text{OIII}]\lambda 4363 \text{ \AA}$  line were obtained from 9 spectra of the sample, for which a direct determination of the electron temperature was performed. Whenever possible, upper limits to the flux in the  $[\text{OIII}]\lambda 4363 \text{ \AA}$  line were computed for each spectrum as 3 times the  $\sigma$  of the flux observed at this wavelength. The electron temperatures derived from the two independent observations of VCC 848 are found to be fairly consistent within the errors.

Reddening-corrected (Whitford 1958) line intensities normalized to  $\text{H}\beta$ , are presented in Table 2 together with the derived flux of  $\text{H}\beta$  (not extinction corrected), and the values of  $C(\text{H}\beta)$  and  $\text{EW}(\text{H}\beta)$  in emission for the sample galaxies. The errors quoted in Table 2 do not include the contribution from the uncertainty in the reddening coefficient.

For the galaxies in common, we have compared our data with previous spectroscopic results in the literature (Gallagher and Hunter 1989, Izotov and Guseva 1989). We find general agreement for the values of  $R_{23}$  derived, especially for the brighter objects: VCC 144, VCC 1725, VCC 1374, VCC 334. For VCC 2033 the match is somewhat poorer, as in the case of VCC 848; this seems to be largely a consequence of the different aperture sizes and position angles of the slit used by the different authors. It is important to point out here that, as shown in Table 3, for the objects in common, the three independent studies give values of  $R_{23}$  which are consistent within the errors, though they were performed in different epochs and with different telescope-spectrograph combinations. In the case of VCC 72 (15deg 9) in the Virgo cluster catalog, its large radial velocity of  $6351 \text{ km s}^{-1}$  (RC3 catalog; confirmed in our spectra) prevent us from including this galaxy in the abundance study of Virgo dwarfs.

### 3.2. Physical Conditions and Abundance Analysis

Electron densities,  $N_e$ , have been derived from the  $[\text{S II}]\lambda\lambda 6717/6731 \text{ \AA}$  ratio using standard algorithms (*e.g.* McCall 1984; Aller 1984). All the regions studied give values typical of low-density H II regions. For the objects in common this result is consistent with previous work (Gallagher and Hunter 1989; Izotov and Guseva 1989).

For those galaxies with  $[\text{OIII}]\lambda 4363 \text{ \AA}$  flux measured, the electron temperature of the high ionization zone,  $t_{[\text{OIII}]}$  was derived using FIVEL (Shaw & Dufour 1995) assuming the low density limit. The temperature of the low ionization zone,  $t_{[\text{OII}]}$ , has been determined assuming its relation with  $t_{[\text{OIII}]}$  from photoionization models (Pagel et al. 1992). For the galaxies VCC 1699 and VCC 144 the  $[\text{SIII}]\lambda 6312 \text{ \AA}$  line was measured; from the ratio of its intensity to the flux of the nebular  $[\text{SIII}]$  lines a value of the  $t_{[\text{SIII}]}$  temperature has been obtained, which appears consistent with  $t_{[\text{OIII}]}$  to within the errors. Although the

appropriate temperature for the [SIII] and [ArIII] lines is better represented by intermediate values between  $t_{[\text{OII}]}$  and  $t_{[\text{OIII}]}$  (Garnett 1992), for the purpose of this paper we have used  $t_{[\text{OIII}]}$  to derive their corresponding abundances.

For the galaxies with a direct determination of the electron temperature, the following ionic and total abundances and abundance ratios:  $\text{O}^{++}/\text{H}^+$ ,  $\text{O}^+/\text{H}^+$ ,  $\text{O}/\text{H}$ ,  $\text{N}^+/\text{O}^+$ ,  $\text{S}^{++}/\text{H}^+$ ,  $\text{S}^+/\text{H}^+$ ,  $\text{S}/\text{H}$ ,  $\text{Ne}^{++}/\text{O}^{++}$ ,  $\text{Ar}^{++}/\text{O}^{++}$  have been computed using FIVEL (Shaw & Dufour 1995) assuming the low density limit, and they are presented in Table 4.

For those galaxies without a direct measurement of a temperature sensitive line, the total abundance of oxygen was derived using a sample of different existing abundance calibrations. The behavior of optical oxygen line intensities in HII regions as a function of oxygen abundance has been studied via semiempirical methods (e.g. Pagel et al. 1979; Alloin et al. 1979; Edmunds & Pagel 1984; Skillman 1989; Zaritsky et al. 1994; Pilyugin 2000) and also using theoretical photoionization models (e.g. Dopita & Evans 1986; McGaugh 1991; Olofsson 1997; Dopita et al. 2000; Charlot & Longhetti 2001).

Several abundance calibrations can be found in the literature that make use of different ratios of relatively bright nebular lines. Among these empirical abundance parameters are  $R_{23}$  (Pagel et al. 1979),  $P$  (Pilyugin 2000) and  $S_{23}$  (Vílchez & Esteban 1996). Additional empirical calibrations make use of the line ratios  $[\text{OIII}]\lambda\lambda 4959,5007/[\text{NII}]\lambda\lambda 6548,84$  (Alloin et al. 1979; Dutil & Roy 1999),  $[\text{NII}]\lambda\lambda 6548,84/H\alpha$  and  $[\text{NII}]\lambda\lambda 6548,84/[\text{OII}]\lambda 3727$  (van Zee et al. 1998).

The optical oxygen lines [OII] and [OIII] are sensitive to both oxygen abundance and electron temperature. At low metallicities, HII region cooling appears dominated by collisional excitation of H Lyman $\alpha$ . Within this regime the total oxygen line intensity increases with abundance. At high metallicities, the oxygen abundance becomes the main coolant, and the cooling is then transferred from the optical to the infrared fine-structure lines [OIII] $\lambda\lambda 52, 88\mu$ . Correspondingly, in this regime the intensities of the optical oxygen lines decline as the oxygen abundance increases.

On this basis, the abundance parameter  $R_{23}$ , defined by Pagel et al. (1979) as  $R_{23} = ([\text{OII}]\lambda 3727 + [\text{OIII}]\lambda\lambda 4959,5007)/H\beta$  has been widely used in the literature as an abundance index. Also from this behavior, the  $12 + \log(\text{O}/\text{H})$  versus  $R_{23}$  abundance calibration results double valued, presenting an ambiguity between the high and low abundance branches, together with a turnover region centered between  $12 + \log(\text{O}/\text{H}) \approx 8.2-8.3$  (e.g. McGaugh 1991, 1994; Miller & Hodge 1996; Oloffson 1997).  $R_{23}$  has been calibrated by different authors (Edmunds & Pagel 1984; McCall et al. 1985; Dopita & Evans 1986; see a comparison in McGaugh 1991). These calibrations might differ systematically at high-metallicity (i.e.



$\log R_{23} < 0$ ) by up to 0.2-0.3 dex, and there are some indications that empirical abundances in this range might be overestimated (e.g. Castellanos et al. 2002; Pilyugin 2001; Kinkel & Rosa 1994; see also Bresolin & Kennicutt 2002). The typical uncertainties quoted for  $R_{23}$  empirical abundances are between 0.1 dex at low metallicity, up to 0.2 dex in the turnover region and the high abundance end.

The parameter  $S_{23}$ , defined as  $S_{23} = ([\text{SII}]\lambda\lambda 6716, 31 + [\text{SIII}]\lambda\lambda 9069, 9532)/\text{H}\beta$  (Vílchez & Esteban 1996) has been calibrated by Díaz & Pérez-Montero (2000) as an empirical abundance index, in analogy to  $R_{23}$ . Spectroscopically, the sulphur lines defining  $S_{23}$  are analogous to the optical oxygen lines in  $R_{23}$  though, given their longer wavelengths, their contribution to the cooling become important at lower temperatures (Díaz & Pérez-Montero 2000). Thus,  $S_{23}$  appear to show a monotonic behavior over a larger range of oxygen abundance. Kennicutt et al. (2000) have found that  $S_{23}$  can show considerable scatter within an HII region and suggested it should be applied to integrated spectra; nonetheless the dispersion they derived in the abundances when using  $S_{23}$  was only slightly larger than in the case of  $R_{23}$ . This calibration can provide more accurate abundances for objects with oxygen abundances between  $12 + \log(\text{O}/\text{H}) = 7.20$  ( $0.02 Z_{\odot}$ ) and  $12 + \log(\text{O}/\text{H}) = 8.80$  ( $0.75 Z_{\odot}$ ) (cf. Díaz & Pérez-Montero 2000).

Pilyugin (2000; 2001) has proposed a new empirical method for the determination of the oxygen abundance in HII regions based on the definition of the parameter  $P = ([\text{OIII}]\lambda\lambda 4959, 5007/\text{H}\beta)/R_{23}$ . Following earlier suggestions by McGaugh (1991) that the strong oxygen lines of  $[\text{OII}]$  and  $[\text{OIII}]$  have enough information for the determination of abundances in H II regions, he compared oxygen abundances in bright HII regions derived from direct determination of the electron temperature, with those derived through the proposed P-method. He has found that the precision of the oxygen abundances derived with the P-method is comparable to the one obtained using a direct determination of the electron temperature. Two abundance relations were obtained: one for low metallicity HII regions, lower than  $12 + \log(\text{O}/\text{H}) \approx 8.1$ , and another one for high metallicity HII regions with  $12 + \log(\text{O}/\text{H}) \geq 8.2$  (i.e. similar to the upper and lower abundance branches of the O/H vs.  $R_{23}$  relationship).

In his theoretical work, McGaugh (1991) produced an extensive grid of HII region models parameterized by the shape of the ionizing spectrum, the geometry of the nebula, and the abundance of the gas. He found that the behavior of the strong oxygen lines can be modeled by taking into account the softening of the ionizing spectra produced by stars of increasing metallicity. In these models, the ratio  $[\text{OIII}]\lambda\lambda 4959, 5007/[\text{OII}]\lambda 3727$  and  $R_{23}$  are used to constrain both, the metallicity and the ionization parameter. The  $[\text{OIII}]/[\text{OII}]$  vs.  $R_{23}$  surface predicted by the models is double valued due to the two cooling regimes described above

operating at high and low abundance. This theoretical calibration appears consistent with recent observations and photoionization models of high abundance objects (e.g. Castellanos et al. 2002 and references therein). It has an estimated mean uncertainty of 0.1 dex. Overall, we should bear in mind that the geometry and aging of the HII regions could introduce some scatter in the calibration (e.g. Stasinska 1999).

Dopita et al. (2000) theoretically have recalibrated the extragalactic H II region sequence and defined the theoretical boundary between HII regions and active galactic nuclei. They used the PEGASE (Fioc & Roca-Volmerange 1997) and STARBURST99 (Leitherer et al. 1999) codes to generate the spectral energy distribution of the ionizing star clusters, and MAPPINGS3 (Sutherland & Dopita 1993) was used to compute photoionization models, including a self-consistent treatment of dust physics and chemical depletion. The extragalactic HII region sequence of observations is well reproduced by these models, assuming that the ionizing clusters are all young ( $\leq 2\text{Myr}$ ) (these authors point out this is likely a selection effect). They proposed that the ratio  $[\text{NII}]\lambda\lambda 6548,6584/[\text{OII}]\lambda 3727$  gives the best diagnostic of abundance, being monotonic between  $0.1 Z_{\odot}$  and over  $3.0 Z_{\odot}$ .

More recently, Charlot and Longhetti (2001) combined recent population synthesis and photoionization codes to compute the line and continuum emission from star-forming galaxies. They calibrate the nebular properties of the models using observations of line ratios for a sample of star-forming galaxies. From optical spectral fits they are able to constrain the star formation history, the gas abundance, and the absorption by dust.

For the determination of abundances in this paper we have used: i) the analytical expression of the McGaugh (1991) theoretical models reported in Kobulnicky et al. (1999); ii) the theoretical calibration of  $[\text{NII}]/[\text{OII}]$  after Dopita et al. (2000); together with iii) the empirical calibration of  $S_{23}$  (Díaz & Pérez-Montero 2000); and iv) the empirical calibration of the parameter P (Pilyugin 2000; 2001). For each galaxy, an average oxygen abundance  $\langle 12+\log(\text{O}/\text{H}) \rangle$ , and its N/O abundance ratio,  $\langle \log(\text{N}/\text{O}) \rangle$ , have been finally adopted. In the next section we discuss the abundance analysis and present the final adopted abundances for the sample galaxies.

#### 4. Discussion and Conclusions

In this work oxygen abundances and N/O abundance ratios have been derived for 21 dwarf galaxies in the Virgo Cluster. These results show that the oxygen abundances of the galaxies span in the metallicity range  $0.04 Z_{\odot} \leq Z \leq 1 Z_{\odot}$ . The nitrogen to oxygen ratios derived ranging from values typical of low metallicity, field BCD galaxies up to near

solar ratios. The oxygen abundance and the nitrogen to oxygen abundance ratios for our Virgo sample are presented in Table 5. Comparison with previous work on abundances of Virgo dwarfs is a difficult task due to the shortage of papers devoted to this subject. Previous spectroscopy of several star-forming Virgo dwarfs has been done by Gallagher & Hunter (1989) and Izotov & Guseva (1989). Bright line ratios, such as  $R_{23}$ , can be derived for some of their objects allowing, in principle, a rough estimation of the abundance to be done. Unfortunately, given the rather poor S/N of the spectra, the faint [NII] lines were not available in previous works, implying a fairly large uncertainty. Only an average value of the oxygen abundance of  $12+\log(\text{O}/\text{H}) \approx 8.2 \pm 0.3$ , is available in Gallagher & Hunter (1989) for their sample of Virgo dwarfs. This abundance was derived using the  $R_{23}$  calibration by Edmunds & Pagel (1984) and is consistent with the range of oxygen abundances derived in this work. For the four galaxies in common with the sample of Izotov & Guseva (1989): VCC 144, VCC 324, VCC 1437 and VCC 2033, the abundances they derived are between  $8.3 \leq 12+\log(\text{O}/\text{H}) \leq 8.5$  with a typical  $1\sigma$  error of 0.26 dex. They have derived abundances using an estimation of the electron temperature for each object using the empirical relation presented in Pagel et al. (1979). These abundance values appear consistent, within the errors, with the values derived in this work for the same objects.

In order to adopt the oxygen abundance,  $\langle 12+\log(\text{O}/\text{H}) \rangle$ , and nitrogen to oxygen abundance ratio,  $\langle \log(\text{N}/\text{O}) \rangle$ , for each galaxy of the sample, we have proceed as follows: i) For the (9) objects with an electron temperature measurement, the abundances derived using the electron temperature, quoted in Table 4, have been adopted and they are presented in Table 5 (In the following, we will refer to these abundances as “direct” abundances).

ii) For each of the (13) remaining objects, an average abundance value, or the corresponding abundance interval, has been finally adopted and is presented in Table 5. This average value for each galaxy was derived from the predictions of the corresponding abundance calibrations used in this work (see Section 3) as it is described below. In this respect, the dispersion among the abundance predictions for each object can be seen as an indicator of the uncertainty in the derivation process. We believe that the advantage of using several calibrations, instead of choosing a single one, is that we can obtain a more realistic estimate of the uncertainty (e.g. Zaritsky et al. 1994).

At this point it is important to emphasize the role that the [NII]/[OII] ratio plays in the abundance calibrations. This line ratio has been shown to be monotonic with oxygen abundance between  $0.2 Z_{\odot}$  up to  $3.0 Z_{\odot}$  (Dopita et al. 2000), a metallicity range where nitrogen behaves as a secondary element. It is also important to bear in mind that the [NII]/[OII] ratio depends on both, electron temperature and N/O abundance ratio. Thus, choosing a different formula accounting for the dependence of N/O on O/H in principle would

lead to different values of the line ratio (e.g. Bresolin et al. 2002 and references therein). For example, Stasinska et al. (2001) models have adopted a mild dependence of N/O on O/H abundance ( $\log(\text{N/O}) = 0.5\log(\text{O/H})+0.4$ ) leading to smaller  $[\text{NII}]/[\text{OII}]$  ratios.

Nevertheless, as originally proposed by Edmunds & Pagel (1978), N/O may also change with time as a consequence of delayed production of nitrogen. This fact may have some relevance in the process of abundance determination, when comparing with the predictions for the zero-age case. Indications of such behavior have been pointed out on the plot of N/O versus O/H for HII regions and star-forming galaxies (e.g. van Zee et al. 1998; Henry et al. 2000) notably for abundances between  $0.1Z_{\odot}$  to  $0.5Z_{\odot}$ . On the other hand, variations in the N/O ratio can also be produced due to the effects of gas inflow or outflow in the galaxy and/or self-enrichment (see Henry et al. 2000). For primary nitrogen, N/O can be affected only in the case of a differential outflow (i.e. different outflow for oxygen than for nitrogen); when nitrogen is secondary, N/O can be affected by an unenriched inflow in addition to the differential outflow (Henry et al. 2000; Koppen and Edmunds 1999, and references therein).

The  $[\text{NII}]/[\text{OII}]$  ratio presents a single parameter sequence from high to low abundances (e.g. van Zee et al. 1998; Dopita et al. 2000). As commonly accepted, in this work we have assumed that those HII regions showing  $\log([\text{NII}]/[\text{OII}]) < -1.0$  present lower oxygen abundances, with respect to those regions with  $\log([\text{NII}]/[\text{OII}]) \geq -1.0$  which correspond to the high abundance regime (e.g. McGaugh 1994; Miller & Hodge 1996; van Zee et al. 1998; Contini et al. 2002). In Table 5 the value of  $\log([\text{NII}]/[\text{OII}])$  has been quoted for each galaxy, together with the parameters  $\log([\text{OIII}]/[\text{OII}])$  and  $\log R_{23}$ . These line ratios are necessary to compute the abundance predictions from the different calibrations used in this work, as described in Section 3.

For each galaxy, in Table 5 we show the abundance predictions for  $12+\log(\text{O/H})$  that have been obtained using the different calibrations. In the Table  $P_{upper}$  and  $P_{lower}$  refer to the lower and upper oxygen abundance, respectively, predicted from the empirical calibration of Pilyugin (2000; 2001);  $R_{23lower}$  and  $R_{23upper}$  are respectively the lower and upper oxygen abundance predicted by McGaugh (1991) theoretical models, computed using the algorithms reported in Kobulnicky et al. (1999); the abundances obtained from the theoretical calibration of the  $[\text{NII}]/[\text{OII}]$  diagnostic in the models of Dopita et al. (2000) are presented; and finally, the abundances predicted by the empirical calibration of  $S_{23}$  after Díaz & Pérez-Montero (2000) are also quoted. We have quoted in the Table all the abundance predictions of the different calibrations for all the objects. However, in the computation of the average abundance only those predictions within the range of application of each calibration (sect. 3) were considered.

As an additional constraint, for the spectra with appropriate S/N, lower limits to O/H

were computed using the measured upper limits to the  $[\text{OIII}]\lambda 4363 \text{ \AA}$  flux. The lower limits to O/H are quoted also in Table 5. This constraint was fulfilled, whenever meaningful, providing information on the abundance regime.

In Figure 3 we present the diagnostic diagram of  $\log([\text{OIII}]/[\text{OII}])$  versus  $\log([\text{NII}]/[\text{OII}])$  with the points of our sample of Virgo galaxies; superposed is the models grid of Dopita et al. (2000) for abundances  $0.2Z_{\odot}$  up to  $2Z_{\odot}$ . Triangles and circles correspond to objects with  $\log([\text{NII}]/[\text{OII}]) < -1.0$  and  $\geq -1.0$  respectively. Filled points represent those objects for which a “direct” determination of the abundance has been obtained. A sequence of points can be seen in the Figure, where the highest abundances, between  $1$  to  $1.5Z_{\odot}$ , are predicted for four objects in the sample. Many points cluster around the  $0.5Z_{\odot}$  line, while only three points –spanning the whole range in ionization parameter,  $\log u$ , in the plot– are consistent with the lowest abundance predictions shown for  $0.2Z_{\odot}$  (according to Figure 6 in Dopita et al. (2000) these points can be consistent also with the locus of the models for  $0.1Z_{\odot}$ ). A comparison between the abundances predicted from these models and the “direct” abundances for the objects in Table 4 tell us that models give abundances which are consistent, within the errors, for the three objects with  $12 + \log(\text{O}/\text{H}) \geq 8.2$ ; the galaxies with “direct” abundances lower than  $0.2Z_{\odot}$  are out of the range allowed for these models.

The  $\log([\text{OIII}]/[\text{OII}])$  versus  $\log R_{23}$  diagnostic diagram is presented in Figures 4 and 5. McGaugh (1991) models, as reported in Kobulnicky et al. (1999), are shown for the lower, Figure 4, and higher, Figure 5, abundance regimes. The points are coded as in Figure 3. Model predictions for the oxygen abundance, increasing by 0.1 dex from  $12 + \log(\text{O}/\text{H}) = 7.4$ , are shown in Figure 4 as continuous lines. In Figure 5, corresponding models are shown from  $12 + \log(\text{O}/\text{H}) = 8.2$  by dotted lines, each line increasing by 0.1 dex. As stated before, triangles represent objects which are to be analyzed using the low abundance models, whereas circles represent objects corresponding to high abundance models. The somewhat larger uncertainty expected in the turnover region, pointed out in Section 3, is apparent when extrapolating model predictions around  $12 + \log(\text{O}/\text{H}) = 8.2$  in both figures. Looking at Figures 4 and 5 and Table 5 we can see that, for most of the objects with a “direct” oxygen abundance, these abundances are consistent with model predictions, within the nominal error of 0.2 dex. It is striking the large discrepancy between model’s and “direct” abundances found for VCC 802, VCC 848 and VCC 1725. For these three galaxies  $R_{23upper}$  has been selected since they show  $\log([\text{NII}]/[\text{OII}]) \geq -1.0$ . However, it is interesting to note that these discrepancies would be minimized adopting  $R_{23lower}$  instead of  $R_{23upper}$ , under the hypothesis that  $[\text{NII}]/[\text{OII}]$  for these galaxies is higher than the value expected for dwarf galaxies with similar oxygen abundance.

A comparison between “direct” and empirical abundances derived using Pilyugin (2000;

2001) for the galaxies in Table 4 give a smaller difference, typically comparable to the nominal error of the calibration. From Table 5 we can notice again the striking cases of VCC802, VCC 848, VCC 1725 for which we find that  $[12 + \log(\text{O}/\text{H}) - P_{upper}] = -0.56, -0.35, -0.66$  dex respectively. As in the case of the  $R_{23}$  McGaugh’s models noted above, if we would assume  $P_{lower}$  instead of  $P_{upper}$  for the three galaxies, these differences would decrease to  $[12 + \log(\text{O}/\text{H}) - P_{upper}] = -0.06, -0.05, -0.26$  dex, giving values closer to the nominal error of the calibration. In the case of VCC 1699 we find  $[12 + \log(\text{O}/\text{H}) - P_{lower}] = 0.45$  dex whereas  $[12 + \log(\text{O}/\text{H}) - P_{upper}] = -0.06$  dex. In this case, since VCC 1699 shows  $\log R_{23} > 0.9$ , it is likely that this point belongs to the turnover region of the calibration and then, as described below, its expected empirical abundance would be consistent with its “direct” abundance.

Both, the  $R_{23}$  and  $P$  abundance calibrations, when  $\log R_{23}$  is larger than 0.9 enter a region around  $12 + \log(\text{O}/\text{H})=8.2$  to 8.3 where abundance predictions are more uncertain (see Sect. 3). This region corresponding to the turnover between low and high abundance branches of both calibrations. At this point, the  $[\text{NII}]/[\text{OII}]$  calibration from the theoretical models of Dopita et al. (2000) begins to work up to oversolar values. Nevertheless, these models for  $0.1Z_{\odot}$  and for  $0.2Z_{\odot}$  predict nearly the same locus in the  $\log([\text{NII}]/[\text{OII}])$  versus  $\log([\text{OIII}]/[\text{OII}])$  diagram (Figure 6 in Dopita et al. 2000). This fact imply, in practice, that objects with abundances between  $7.9 \geq 12 + \log(\text{O}/\text{H}) \geq 8.2$  would not be discriminated. Thus, we have adopted a somewhat conservative approach assuming an average abundance of  $12 + \log(\text{O}/\text{H}) \approx 8.2$ , with a 0.2 dex error bar, for those objects in the sample without a direct abundance determination and presenting  $\log R_{23}$  larger than 0.9.

The  $S_{23}$  parameter seems to be monotonic across this abundance region, but it was available only for two of the objects of the Virgo sample: VCC 144 and VCC 1699. For these two galaxies, as can be seen in Table 5, the oxygen abundances provided by the  $S_{23}$  calibration (Díaz & Pérez-Montero 2000) are in good agreement with the “direct” abundances, within the nominal error of the calibration.

For some of the objects without a “direct” abundance we have adopted an interval in  $12 + \log(\text{O}/\text{H})$  with the aim of encompassing the range in  $\text{O}/\text{H}$  predictions (typically between the McGaugh’s and Pilyugin’s calibrations).

The average  $\text{N}/\text{O}$  abundance ratio,  $\langle \log(\text{N}/\text{O}) \rangle$ , has been derived for each galaxy of the sample. In doing that, an “average” electron temperature was assumed for each object, corresponding to the temperature for which the derived oxygen abundance can be reproduced from the observed  $[\text{O III}]$  and  $[\text{O II}]$  fluxes within the errors. From photoionization models, it is well known that for temperatures  $t_{[\text{OIII}]} \geq 1.2$  K,  $t_{[\text{OIII}]}$  is higher than  $t_{[\text{OII}]}$  and the opposite is found for  $t_{[\text{OIII}]}$  below this value (e.g. Peimbert 2002 and references therein). Using an average temperature would introduce an error when deriving the nitrogen to oxygen ratio

(e.g. van Zee et al. 1998). Assuming a typical difference of 1.000 K between  $t_{[\text{OIII}]}$  and  $t_{[\text{OII}]}$  within the average temperature range used, would imply a typical error of 0.06 dex in  $\langle \log(\text{N/O}) \rangle$ , which we believe is within the nominal error budget of the calibrations.

The use of strong line diagrams, notably at high abundance, is subject to large uncertainties (see Stasinska 1999 for a review). McGaugh’s (1991) models assume unevolving ionizing stellar clusters, whereas it is known that both, the ionization parameter as well as the shape of the ionizing spectrum may evolve (e.g. Stasinska & Leitherer 1996; Olofsson 1997). The effect of cluster evolution on the oxygen line fluxes is expected to be important especially at high metallicity, where diagnostic diagrams could change as a function of time (e.g. Stasinska 1999). On the other hand, using the best empirical fit to the samples of abundances derived from temperature-sensitive lines, as in Pilyugin’s P calibration, could lead to lower values of oxygen especially at high abundance (e.g. Stasinska 2002).

There have been some suggestions that the  $R_{23}$  calibration may provide abundances systematically higher by some 0.2-0.3 dex in the high abundance regime, probably depending on the excitation conditions (e.g. Castellanos et al. 2002; Pilyugin 2001; Kinkel & Rosa 1994; see also Bresolin & Kennicutt 2002). The effect of excitation was been taken into account by McGaugh (1991), Pilyugin (2000) and Dopita et al. (2000). For two of the objects showing  $[\text{NII}]/[\text{OII}] \geq 0.1$ , their errors could allow the lower branch to be chosen at the one sigma level, in these two cases, VCC 562 and VCC 2033, the lower branch of  $12 + \log(\text{O/H})$  has been also indicated in Table 5.

For all the objects with  $12 + \log(\text{O/H}) \leq 8.2$  the nitrogen to oxygen ratios derived present values typical of low abundance dwarf galaxies. There are two notable exceptions to this behavior, which deserve independent confirmation and further study: VCC 1725 and VCC 802. Our data for these two objects indicate oxygen abundances below 0.1 solar but their N/O values appear somewhat higher, close to the Orion value of  $\log(\text{N/O}) = -0.85 \pm 0.10$  (Esteban et al. 1998). Among the galaxies with  $12 + \log(\text{O/H}) \geq 8.2$ , a significant fraction present high abundances with O/H and N/O near to or larger than the solar values of  $12 + \log(\text{O/H}) = 8.71 \pm 0.05$  and  $\log(\text{N/O}) = -0.78 \pm 0.12$  (Holweger 2001; Allende Prieto et al. 2001).

Finally, near 50% of the galaxies of the sample present oxygen abundances in between the abundance of the Large Magellanic Cloud,  $12 + \log(\text{O/H}) = 8.39 \pm 0.12$  (Pagel et al. 1978), and that of Orion,  $12 + \log(\text{O/H}) = 8.64 \pm 0.06$  (Esteban et al. 1998). Most of the galaxies presenting the larger O/H abundances or higher N/O ratios tend to be associated with spectra showing an important continuum contribution and conspicuous absorption lines. These outstanding objects deserve further study; in particular, following the suggestion that the N/O ratio could indicate the time since the bulk of star formation has occurred (Edmunds

& Pagel 1978; Matteucci & Tosi 1985), those objects presenting the highest nitrogen to oxygen ratio we believe could be good candidates to host post-starburst galaxies. Therefore these objects may provide interesting hints for chemical evolution modeling of dwarf galaxies in dense environments.

A detailed study of the results obtained in this work will be presented in paper II. In the framework of the metallicity-(mass)-luminosity relation (Skillman et al. 1989; Richer et al. 1998; Hidalgo-Gómez & Olofsson 1998; Pilyugin 2001) paper II is aimed to analyze the relationship between metallicity and the fundamental properties and chemical evolution of Virgo dwarf galaxies.

The WHT is operated on the island of La Palma by the ING in the Spanish Observatorio del Roque de Los Muchachos of the Instituto de Astrofísica de Canarias. We acknowledge CAT for the allocation of telescope time to this project. We thank an anonymous referee for many interesting suggestions and comments which have helped to improve this paper. JMV thanks the I.A.C. (Tenerife) and the L.A.S. (Marseille) for hospitality and partial funding during the realization of this work. JMV acknowledges financial support from a CSIC “Marina Bueno” grant. JIP acknowledges a European “Marie Curie” Fellowship. This research is supported by project AYA2001-3939-C03-01 of the Spanish Plan Nacional de Astronomía y Astrofísica.



## REFERENCES

- Allende Prieto, C., Lambert, D. L., & Asplund, M. 2001, *ApJ*, 556, L63
- Aller, L. H. 1984, *Physics of Thermal Gaseous Nebulae*, 1984 *Astrophysics & Space Science Library* vol. 112
- Alloin, D., Collin-Souffrin, S., Joly, M., & Vigroux, L. 1979, *A&A*, 78, 200
- Binggeli, B., Sandage, A., & Tammann, G. A. 1985, *AJ*, 90, 1681
- Binggeli, B., Tammann, G. A., & Sandage, A. 1987, *AJ*, 94, 251
- Boselli, A., Gavazzi, G., Lequeux, J., Buat, V., Casoli, F., Dickey, J., & Donas, J. 1997, *A&A*, 327, 522
- Boselli, A., Iglesias-Páramo, J., Vílchez, J. M., & Gavazzi, G. 2002, *A&A*, 386, 134
- Bresolin, F., & Kennicutt, R. C. 2002, *ApJ*, in press astro-ph/0202383
- Brosch, N., Almoznino, E., & Hoffman, G. L. 1998, *A&A*, 331, 873
- Charlot, S. & Longhetti, M. 2001, *MNRAS*, 323, 887
- Castellanos, M., Díaz, A. I., & Terlevich, E. 2002, *MNRAS*, 329, 315
- Cayatte, V., van Gorkom, J. H., Balkowski, C., & Kotanyi, C. 1990, *AJ*, 100, 604
- Contini, T., Treyer, M. A., Sullivan, M., & Ellis, R. S. 2002, *MNRAS*, 330, 75
- Díaz, A. I. & Pérez-Montero, E. 2000, *MNRAS*, 312, 130
- Dopita, M. A. & Evans, I. N. 1986, *ApJ*, 307, 431
- Dopita, M. A., Kewley, L. J., Heisler, C. A., & Sutherland, R. S. 2000, *ApJ*, 542, 224
- Duc, P.-A. & Mirabel, I. F. 1999, *IAU Symp. 186: Galaxy Interactions at Low and High Redshift*, 186, 61
- Dutil, Y. & Roy, J. 1999, *ApJ*, 516, 62
- Edmunds, M. G. & Pagel, B. E. J. 1978, *MNRAS*, 185, 77P
- Edmunds, M. G. & Pagel, B. E. J. 1984, *MNRAS*, 211, 507
- Esteban, C., Peimbert, M., Torres-Peimbert, S., & Escalante, V. 1998, *MNRAS*, 295, 401

- Fioc, M. & Rocca-Volmerange, B. 1997, *A&A*, 326, 950
- Gallagher, J. S. & Hunter, D. A. 1984, *ARA&A*, 22, 37.
- Gallagher, J. S. & Hunter, D. A. 1989, *AJ*, 98, 806
- Garnett, D. R. 1992, *AJ*, 103, 1330
- Gavazzi, G., Boselli, A., Mayer, L., Iglesias-Páramo, J., Vílchez, J. M., & Carrasco, L. 2001, *ApJ*, 563, L23
- Grogin, N. A. & Geller, M. J. 2000, *AJ*, 119, 32
- Hashimoto, Y., Oemler, A. J., Lin, H., & Tucker, D. L. 1998, *ApJ*, 499, 589
- Haynes, M. P., Giovanelli, R., & Chincarini, G. L. 1984, *ARA&A*, 22, 445
- Henry, R. B. C., Edmunds, M. G., & Köppen, J. 2000, *ApJ*, 541, 660
- Hidalgo-Gómez, A. M. & Olofsson, K. 1998, *A&A*, 334, 45
- Hoffman, G. L., Helou, G., & Salpeter, E. E. 1988, *ApJ*, 324, 75
- Holweger, H. 2001, Joint SOHO/ACE workshop "Solar and Galactic Composition", 23
- Hummer, D. G. & Storey, P. J. 1987, *MNRAS*, 224, 801
- Iglesias-Páramo, J. & Vílchez, J. M. 1999, *ApJ*, 518, 94
- Iglesias-Páramo, J., Boselli, A., Cortese, L., Vílchez, J.M., & Gavazzi, G. 2002, *A&A*, 384, 383
- Izotov, Y. I. & Guseva, N. G. 1989, *Astrofizika*, 30, 564
- Kenney, J. D. & Young, J. S. 1988, *ApJS*, 66, 261
- King, D. 1985, La Palma Tech. Note, 15
- Kinkel, U. & Rosa, M. R. 1994, *A&A*, 282, L37
- Kobulnicky, H. A., Kennicutt, R. C., & Pizagno, J. L. 1999, *ApJ*, 514, 544
- Köppen, J. & Edmunds, M. G. 1999, *MNRAS*, 306, 317
- Lee, H., Richer, M. G., & McCall, M. L. 2000, *ApJ*, 530, L17
- Leitherer, C. et al. 1999, *ApJS*, 123, 3

- McCall, M. L. 1984, MNRAS, 208, 253
- McCall, M. L., Rybski, P. M., & Shields, G. A. 1985, ApJS, 57, 1
- McGaugh, S. S. 1991, ApJ, 380, 140
- McGaugh, S. S. 1994, ApJ, 426, 135
- Miller, B. W. & Hodge, P. 1996, ApJ, 458, 467
- Olofsson, K. 1997, A&A, 321, 29
- Pagel, B. E. J., Edmunds, M. G., Blackwell, D. E., Chun, M. S., & Smith, G. 1979, MNRAS, 189, 95
- Pagel, B. E. J., Simonson, E. A., Terlevich, R. J., & Edmunds, M. G. 1992, MNRAS, 255, 325
- Peimbert, M. 2002, Revista Mexicana de Astronomia y Astrofisica Conference Series, 12, 275
- Pilyugin, L. S. 2000, A&A, 362, 325
- Pilyugin, L. S. 2001, A&A, 374, 412
- Popescu, C. C., Hopp, U., & Rosa, M. R. 1999, A&A, 350, 414
- Richer, M., McCall, M. L., & Stasinska, G. 1998, A&A, 340, 67
- Sandage, A. 1961, Hubble Atlas of Galaxies, Carnegie Institution of Washington Publication 618
- Sandage, A., & Tammann, G. A. 1981, Revised Shapley-Ames Catalog of Bright Galaxies, Carnegie Inst. of Washington, Publ. 635
- Sandage, A. & Binggeli, B. 1984, AJ, 89, 919.
- Shaw, R. A. & Dufour, R. J. 1995, PASP, 107, 896
- Sinclair, J. 1996, La Palma Tech. Note, 100
- Skillman, E. D. 1989, ApJ, 347, 883
- Skillman, E. D., Kennicutt, R. C., & Hodge, P. W. 1989, ApJ, 347, 875

- Solanes, J. , Manrique, A., García-Gómez, C., González-Casado, G., Giovanelli, R., & Haynes, M. P. 2001, *ApJ*, 548, 97
- Stasinska, G. 1999, in “Dwarf Galaxies and Cosmology”, ed. T.X. Thuan, C. Balkowsky, V. Cayatte, J.T. Than Van (Editions Frontieres), 259
- Stasińska, G., Schaerer, D., & Leitherer, C. 2001, *A&A*, 370, 1
- Sutherland, R. S. & Dopita, M. A. 1993, *ApJS*, 88, 253
- van Zee, L., Salzer, J. J., & Haynes, M. P. 1998, *ApJ*, 497, L1
- van Zee, L., Salzer, J. J., Haynes, M. P., O’Donoghue, A. A., & Balonek, T. J. 1998, *AJ*, 116, 2805
- Vigroux, L., Lachieze-Rey, M., Thuan, T. X., & Vader, J. P. 1986, *AJ*, 91, 70
- Vílchez, J. M. 1995, *AJ*, 110, 1090
- Vílchez, J. M. 1999, in *Chemical Evolution from Zero to High Redshift* , 175
- Vílchez, J. M. & Esteban, C. 1996, *MNRAS*, 280, 720
- Whitford, A. E. 1958, *AJ*, 63, 201
- Zaritsky, D., Kennicutt, R. C., & Huchra, J. P. 1994, *ApJ*, 420, 87

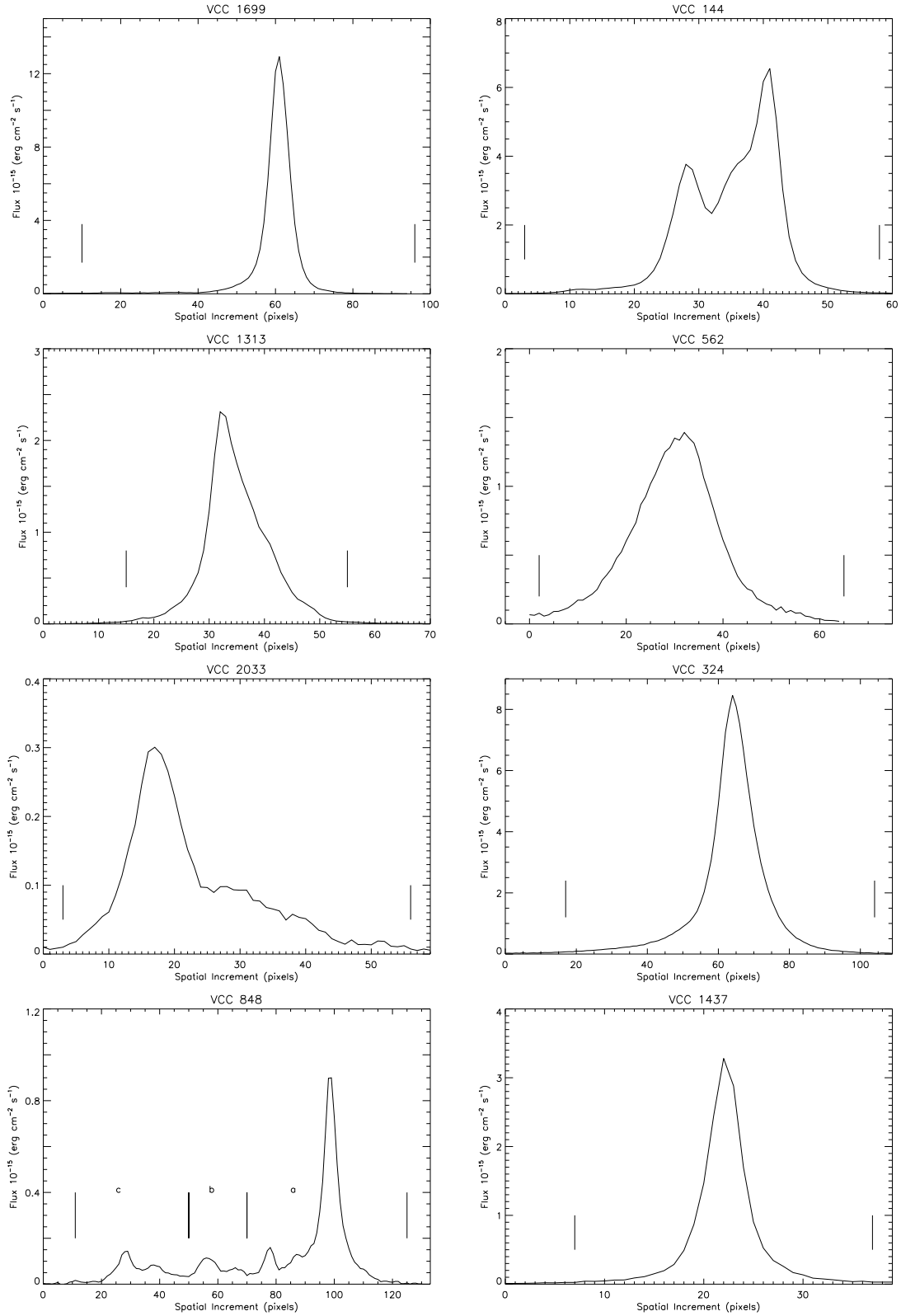


Fig. 1.— Spatial emission profiles of the sample galaxies in a wavelength window centered in H $\alpha$ . The spatial scale is  $0.335'' \text{ pixel}^{-1}$ .

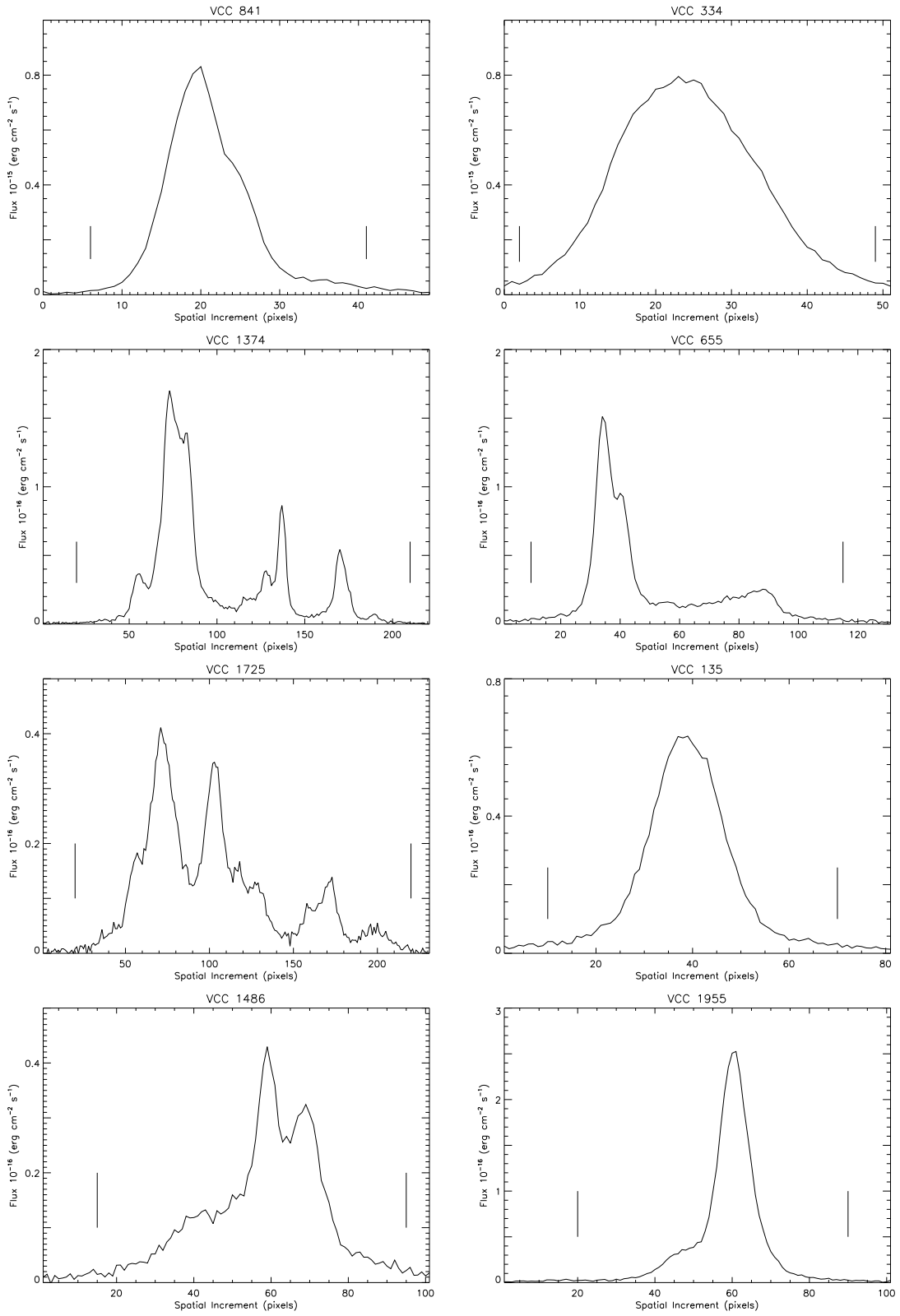


Fig. 1.— Continued.

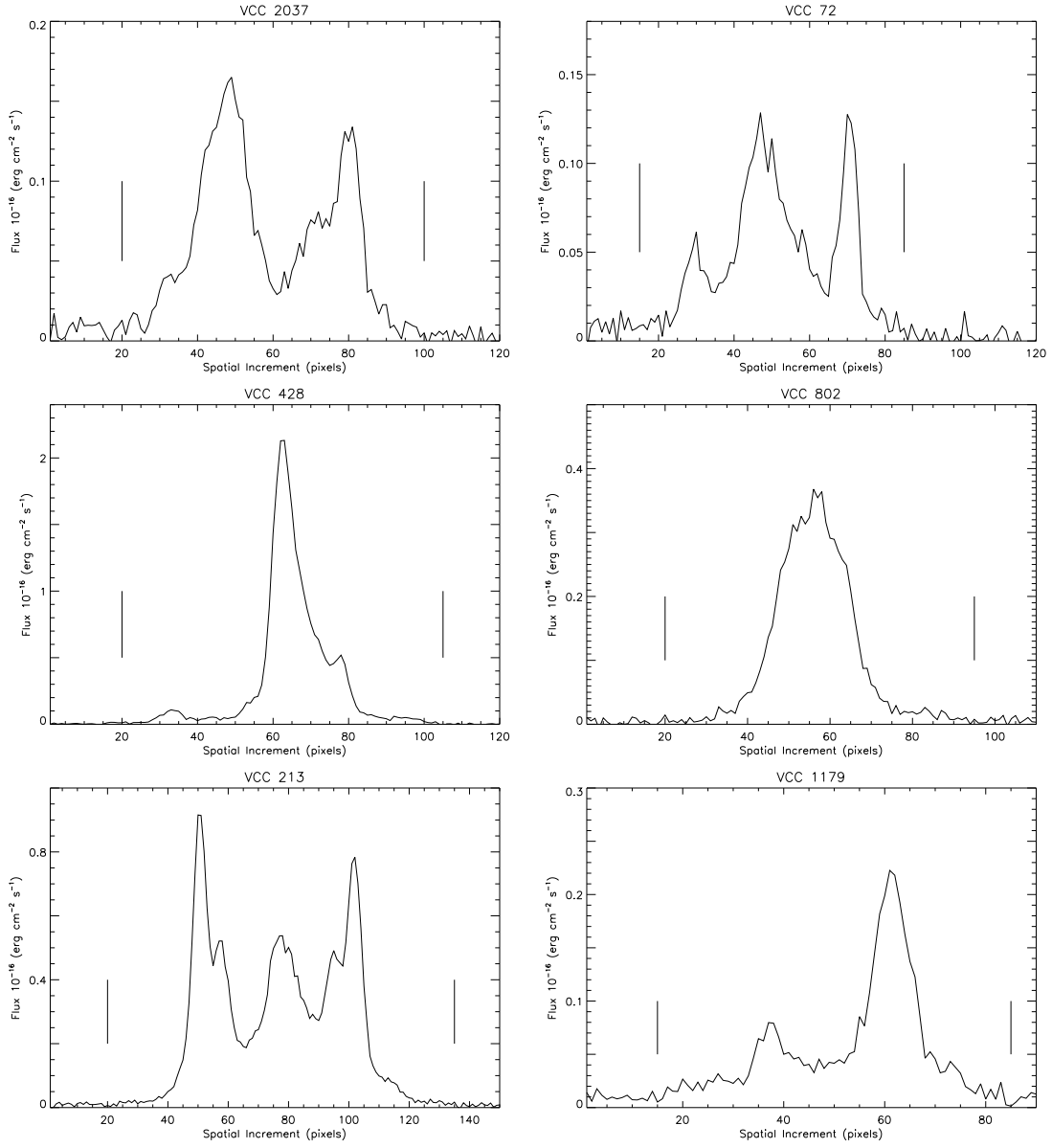


Fig. 1.— Continued.

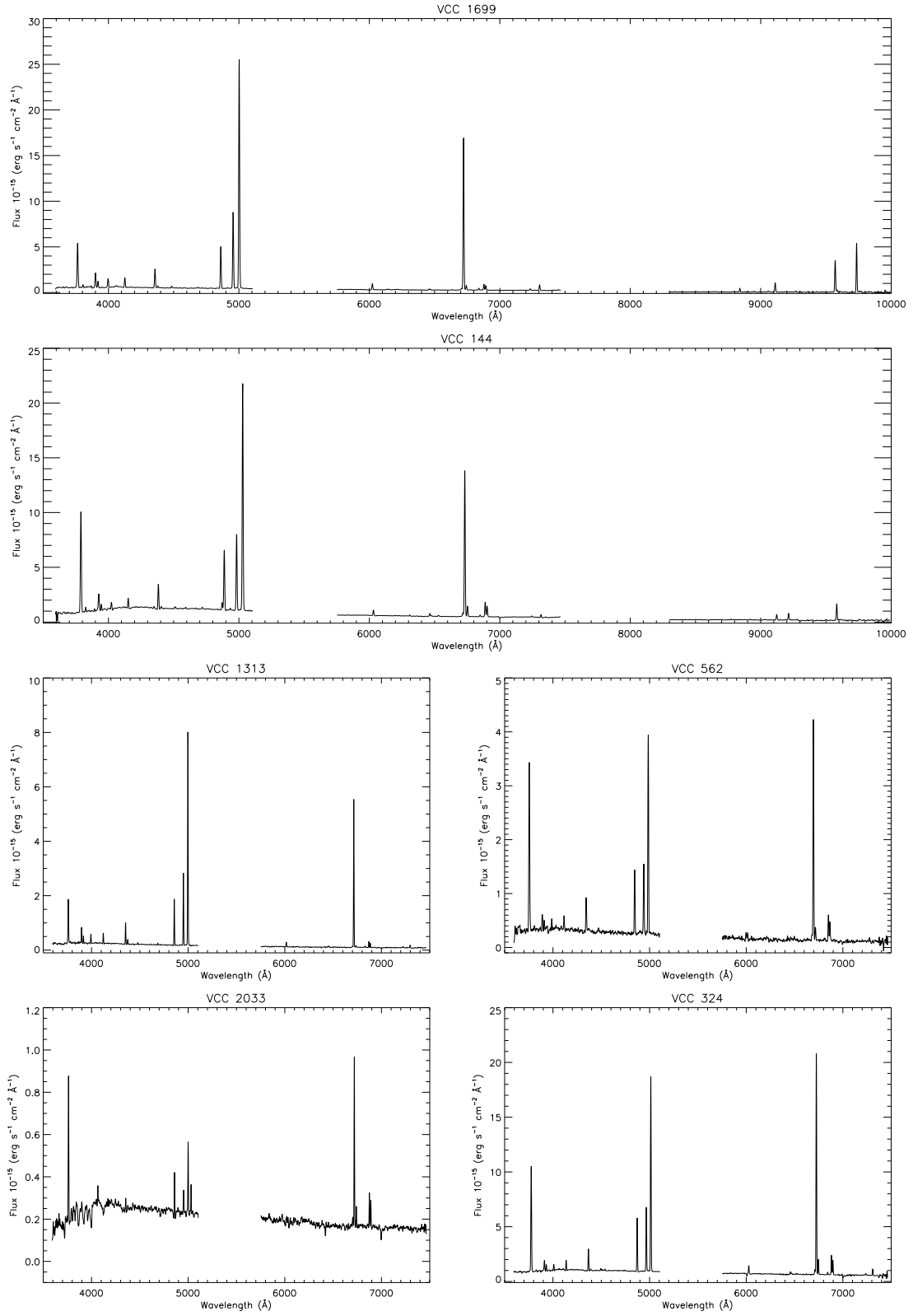


Fig. 2.— Spectra of the galaxies of the Virgo sample.



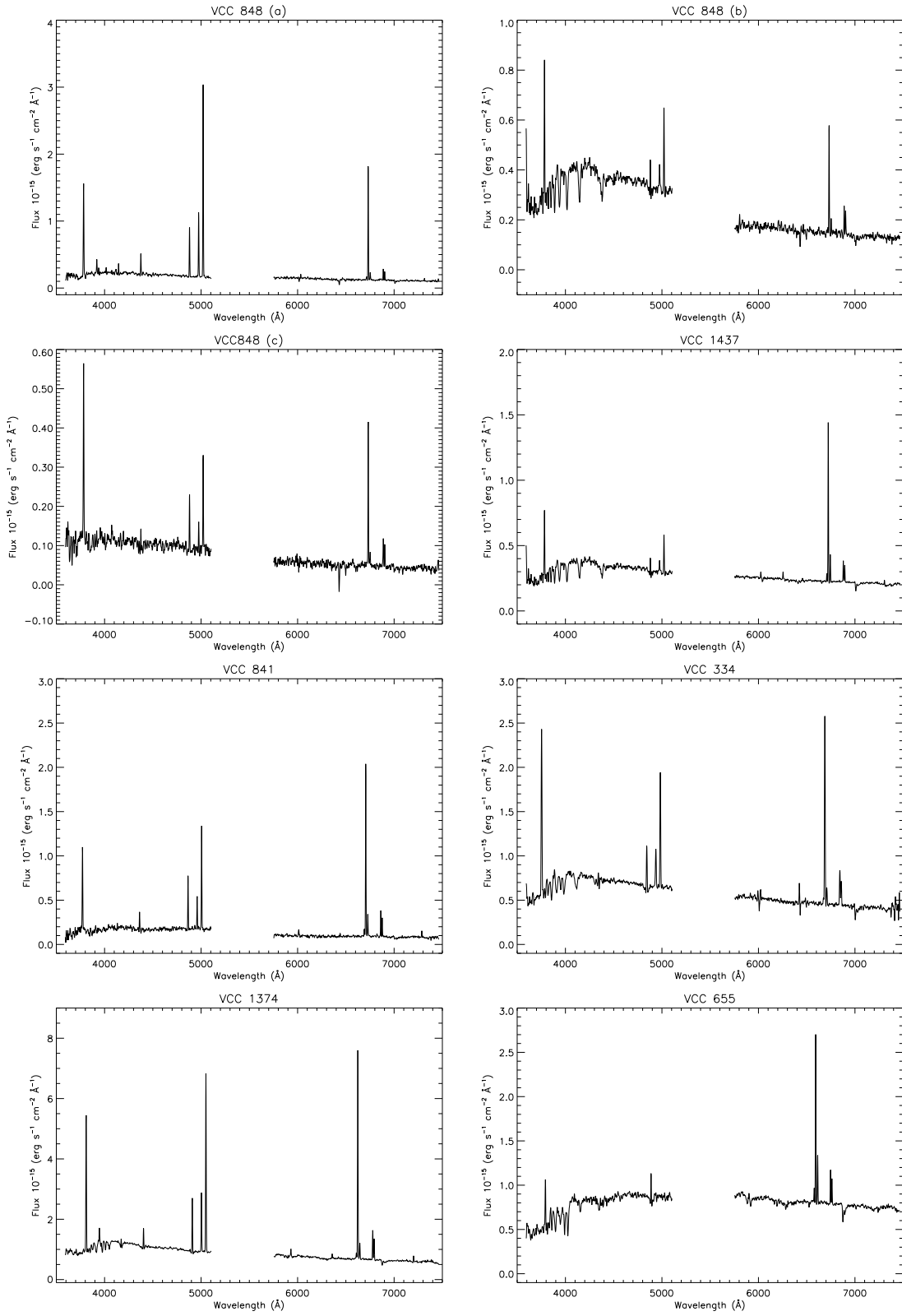


Fig. 2.— Continued.

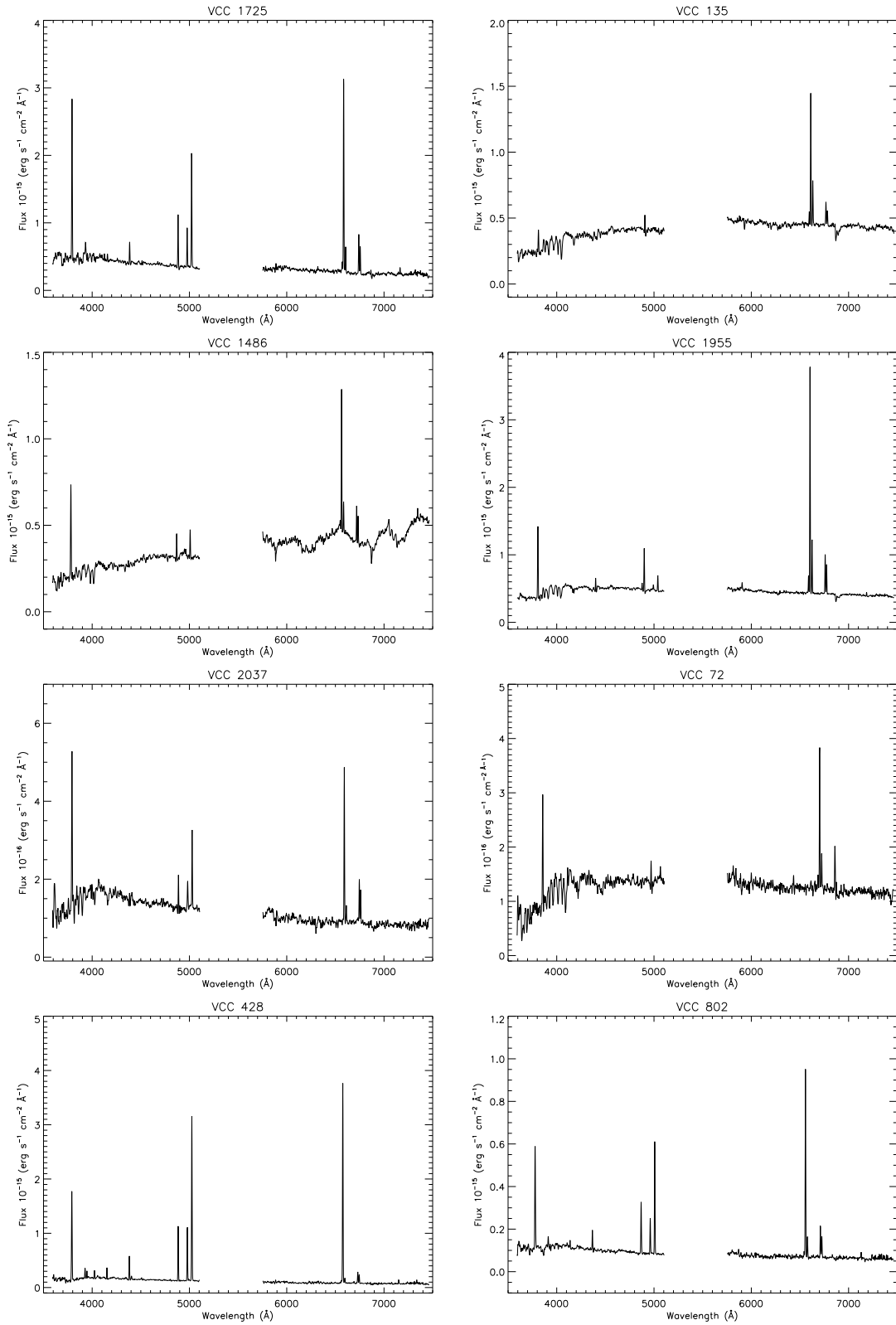


Fig. 2.— Continued.

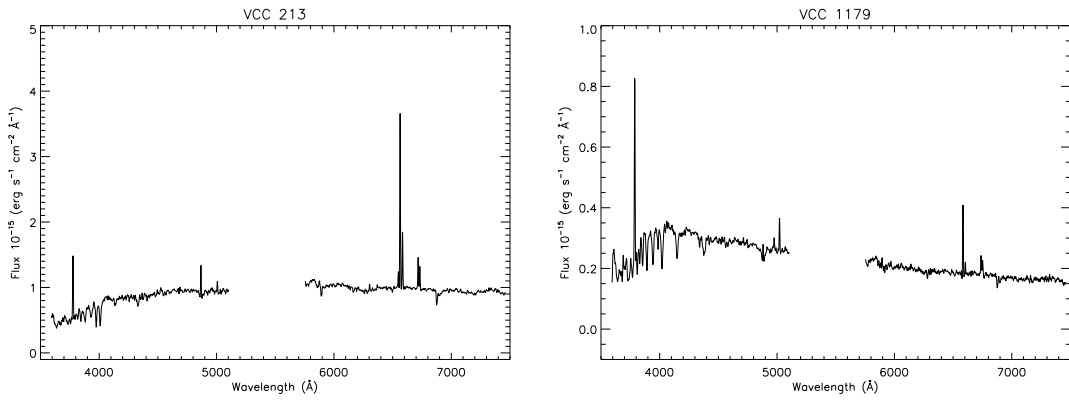


Fig. 2.— Continued.

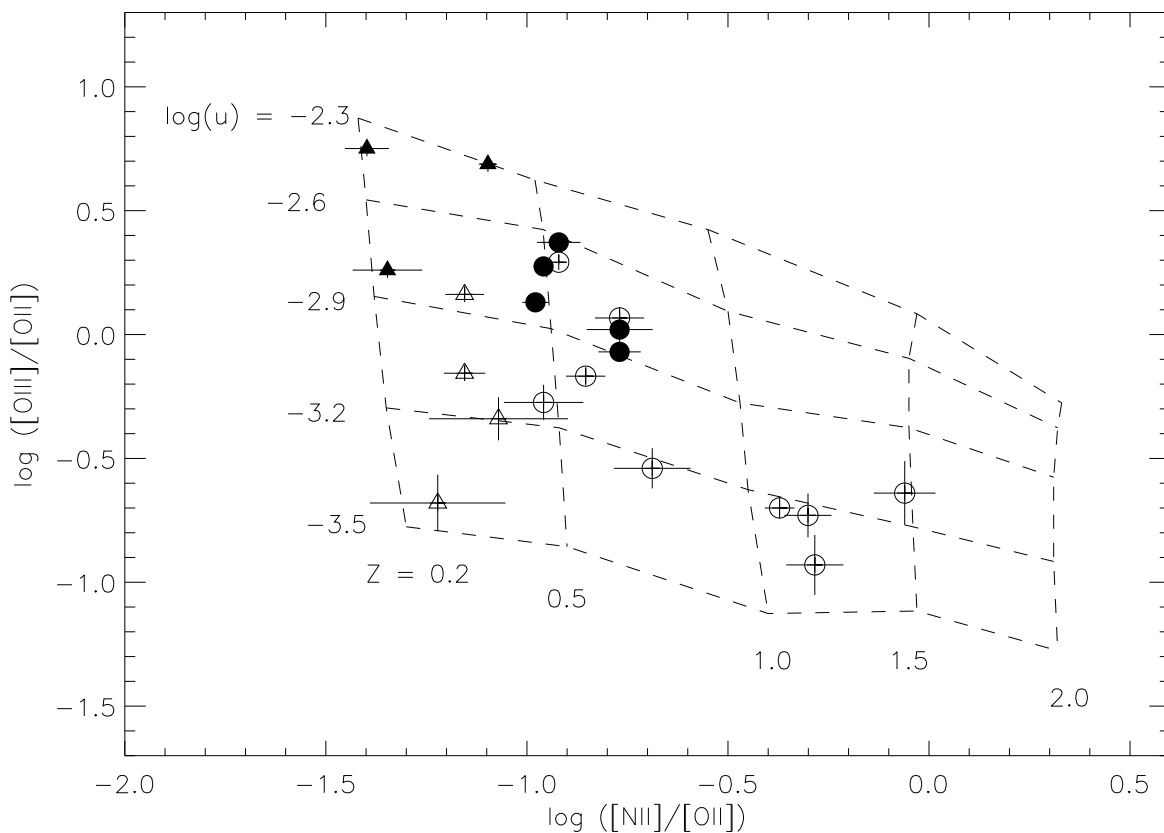


Fig. 3.— Diagnostic diagram  $\log([\text{OIII}]/[\text{OII}])$  vs.  $\log([\text{NII}]/[\text{OII}])$  with the model grid of Dopita et al. (2000) superposed for abundances  $0.2Z_{\odot}$  up to  $2Z_{\odot}$ . Points represent the Virgo galaxies studied here coded as follows: triangles correspond to objects with  $\log([\text{NII}]/[\text{OII}]) < -1.0$ ; circles correspond to objects with  $\log([\text{NII}]/[\text{OII}]) \geq -1.0$ . Filled points represent objects with a “direct” determination of abundance. See the text for details.

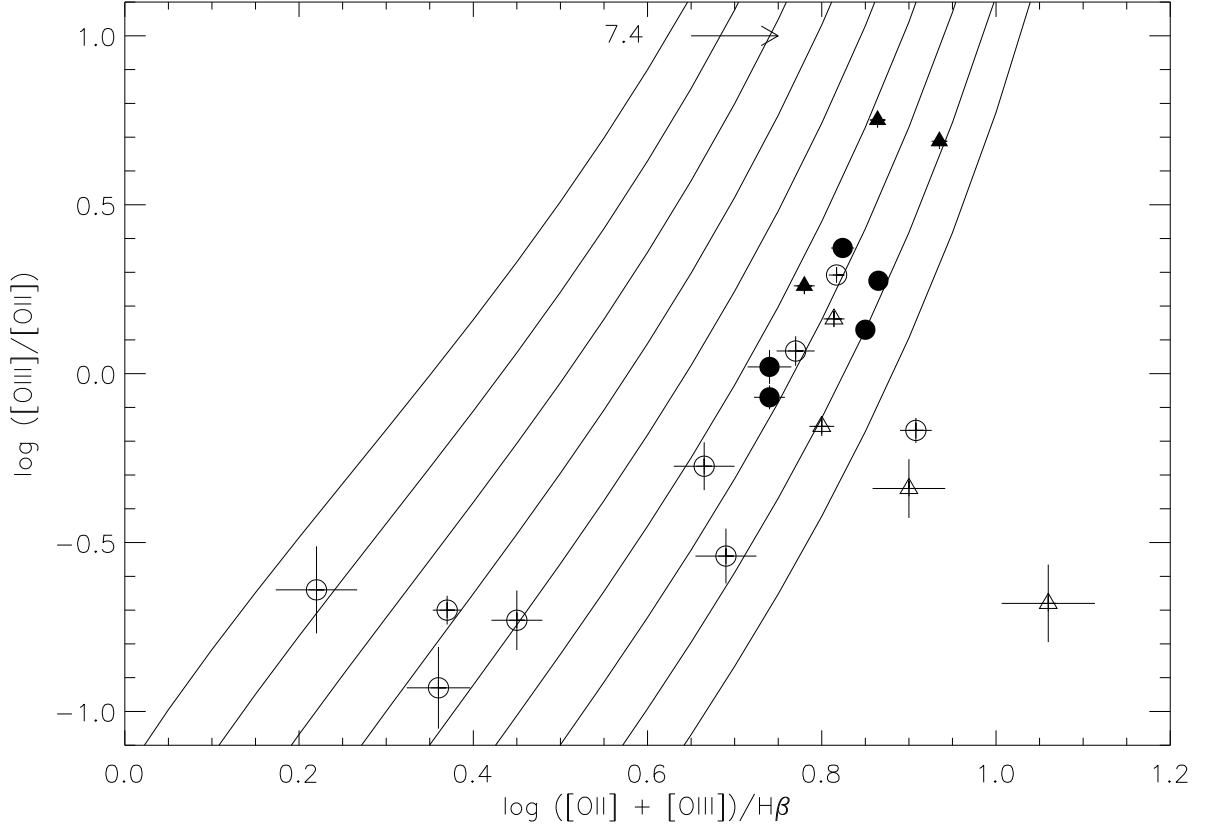


Fig. 4.—  $\log([\text{OIII}]/[\text{OII}])$  vs.  $\log R_{23}$  diagnostic diagram with McGaugh (1991) models, as reported in Kobulnicky et al. (1999), shown as continuous lines. Each line correspond to an oxygen abundance, starting at  $12 + \log(\text{O}/\text{H}) = 7.4$  –marked for the first line to the left– each line increasing to the right in the plot by 0.1 dex. Points are coded as in Figure 3. Triangles represent sample objects corresponding to the low abundance models shown in this figure; while circles represent objects to be analyzed with models for higher abundances as shown in Figure 5 .

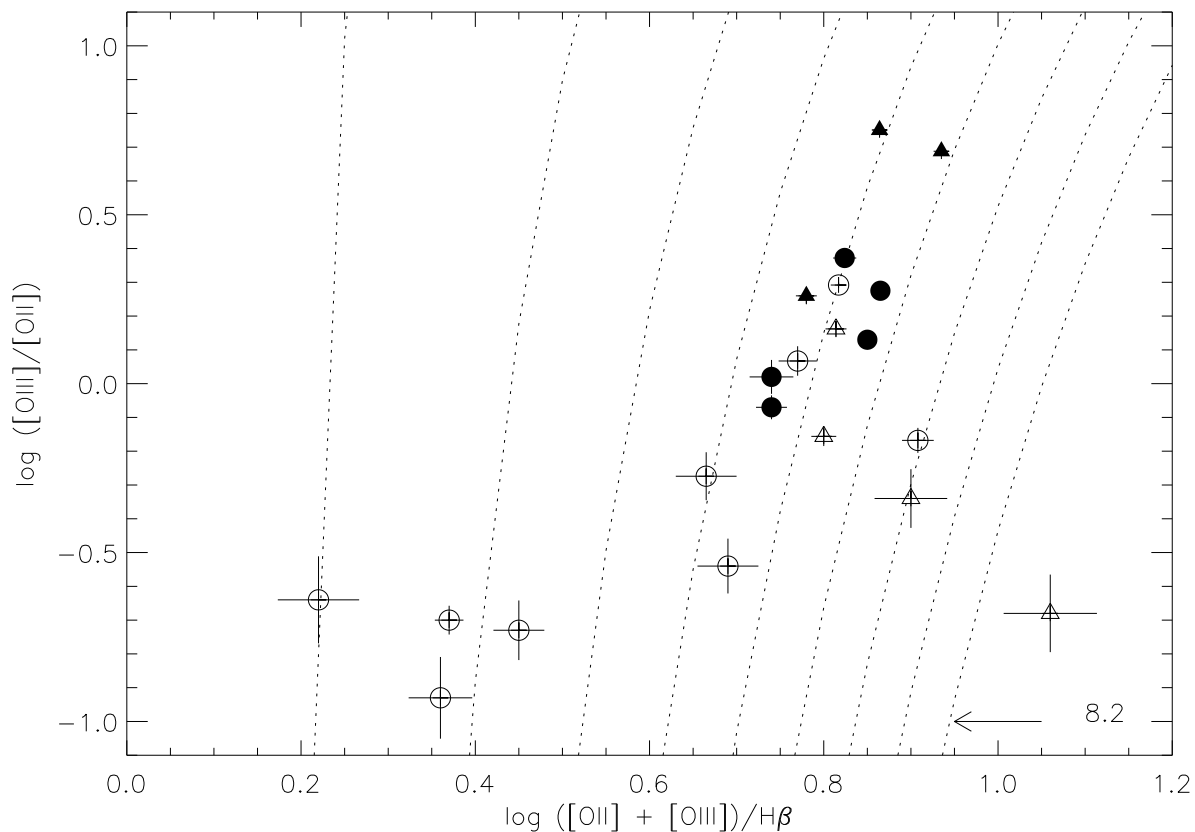


Fig. 5.—  $\log([\text{OIII}]/[\text{OII}])$  vs.  $\log R_{23}$  diagnostic diagram. McGaugh (1991) models, as reported in Kobulnicky et al. (1999), are shown as dotted lines. Each line correspond to an oxygen abundance, starting at  $12 + \log(\text{O}/\text{H}) = 8.2$  –marked for the first line to the right– each line and increasing to the left in the plot by 0.1 dex. Points are coded as in Figure 3. Circles represent sample galaxies corresponding to the high abundance models shown in this figure. Triangles represent objects to be analyzed with models for lower abundances as shown in Figure 4 .

Table 1. Journal of the Observations. (1) VCC name. (2) Other name. (3) Type (4),(5) 1950 coordinates. (6) Position Angle of the slit. (7) Central wavelength of the observation. (8) Exposure time. (9) Date of the observation.

VCC	Other name	Type ( <i>hh mm ss</i> )	$\alpha$ (1950) ( $^{\circ}$ ' ")	$\delta$ (1950) ( $^{\circ}$ )	Pos.Ang. ( $\text{\AA}$ )	$\lambda_c$ (s)	Exposure	Date
1699	IC 3591	SBmIII	12 34 30.3	07 12 10	237	4228	1400	1993 May 25
						4228	1300	1993 May 26
						6448	1300	1993 May 25
						9100	1600	1993 May 26
144	Haro 6	BCD	12 12 45.1	06 02 24	310	4228	2400	1993 May 25
						6448	2300	1993 May 25
						4223	1800	1993 May 26
						9096	1800	1993 May 26
1313	RMB 132	BCD	12 28 16.6	12 19 20	266	4228	2400	1993 May 25
						6448	2400	1993 May 25
562	RMB 175	BCD	12 20 03.3	12 26 05	138	4228	3400	1993 May 24
						6448	3000	1993 May 24
2033	A 1243+08	BCD	12 43 32.8	08 45 02	237	4228	1183	1993 May 25
						4228	1400	1993 May 26
						6448	1162	1993 May 25
324	Mkn 49	Epec/BCD	12 16 36.6	04 07 59	3	4228	2200	1993 May 24
						6448	2100	1993 May 24
848	A 1223+06	ImIIIpec/BCD	12 23 19.5	06 05 11	24	4223	2400	1993 May 26
						6445	2300	1993 May 26
			12 23 19.6	06 05 09		4382	1700	1994 March 11
1437	A 1230+09	BCD	12 30 01.5	09 26 58	57	6549	1600	1994 March 11
						4223	1800	1993 May 26
						6445	1700	1993 May 26
841	RMB 46	BCD	12 23 15.9	15 13 45	344	4223	1800	1993 May 26
						6445	1700	1993 May 26
334	RMB 56	BCD	12 16 41.7	12 26 05	3	4228	2000	1993 May 24
						6448	1900	1993 May 24
1374	IC 3453	IBm/BCD	12 31 37.8	14 51 38	345	4382	1400	1994 March 10
						6549	1300	1994 March 10
655	NGC 4344	SpN/BCD amorph.	12 23 37.5	17 32 27	69	4382	1600	1994 March 10
						6549	1500	1994 March 10
1725	A1235+08	SmIII/BCD	12 37 41.2	08 33 33	116.5	4382	1400	1994 March 12
						6549	1300	1994 March 12
135	IC 3063	S pec/BCD	12 15 06.7	12 01 01	20.5	4382	1243	1994 March 12
						6549	1229	1994 March 12
1486	IC 3483	S pec?,N	12 30 38.1	11 37 22	170.5	4382	1400	1994 March 12
						6549	1300	1994 March 12

Table 1—Continued

VCC	Other name	Type ( <i>hh mm ss</i> )	$\alpha$ (1950) ( $^{\circ}$ ' ")	$\delta$ (1950) ( $^{\circ}$ )	Pos.Ang. ( $\text{\AA}$ )	$\lambda_c$ (s)	Exposure	Date
1955	NGC 4641	Spec/BCD amorph.	12 43 97.6	12 03 03	28	4382 6549	1400 1300	1994 March 12 1994 March 12
2037	10 $^{\circ}$ 71	ImIII/BCD	12 46 15.3	10 12 12	156	4382 6549	1800 1700	1994 March 11 1994 March 11
72	15 $^{\circ}$ 9	ImIII/BCD	12 13 02.0	14 55 58	134.5	4382 6549	1800 1700	1994 March 10 1994 March 10
428	BB 18	BCD	12 20 40.2	13 53 20	29	4382 6549	1500 1500	1994 March 11 1994 March 11
802	BO 146	BCD	12 25 28.7	13 29 50	61.9	4382 6549	1800 1700	1994 March 11 1994 March 11
213	IC 3094	dS?/BCD? amorph.	12 16 56.0	13 37 33	90	4382 6549	1600 1500	1994 March 11 1994 March 11
1179	IC 3412	ImIII/BCD	12 29 22.6	09 59 17	18	4382 6549	1700 1600	1994 March 11 1994 March 11



Table 2. Reddening corrected line intensities relative to  $H\beta$  for the sample of Virgo dwarf galaxies. The reddening coefficient,  $C(H\beta)$ , the equivalent width of  $H\beta$ ,  $EW(H\beta)$  ( $\text{\AA}$ ), and the measured  $H\beta$  flux,  $F(H\beta)$  in units  $10^{-15} \text{ erg cm}^{-2} \text{ s}^{-1}$ , are included. Balmer lines were corrected from underlying stellar absorption. Errors quoted in parenthesis.

Line	$\lambda(\text{\AA})$	$f(\lambda)$	VCC 1699	VCC 144	VCC 1313	VCC 562	VCC 2033	VCC 324
[O II]	3727	0.26	1.260 (0.018)	2.541 (0.031)	1.102 (0.032)	2.656 (0.076)	3.016 (0.232)	2.215 (0.024)
H12	3751	0.20	0.019 (0.001)	—	—	—	—	—
H11	3770	0.26	0.033 (0.002)	—	—	—	—	—
H10	3798	0.25	0.042 (0.002)	—	—	—	—	—
H9	3835	0.24	0.067 (0.003)	—	—	—	—	—
[Ne III]	3868	0.23	0.364 (0.007)	0.270 (0.006)	0.338 (0.014)	—	—	0.183 (0.005)
H8 +He I	3889	0.22	0.177 (0.004)	0.154 (0.005)	0.167 (0.010)	0.100 (0.012)	—	0.109 (0.003)
H $\epsilon$ +[Ne III]	3969	0.21	0.264 (0.005)	0.194 (0.005)	—	—	—	0.132 (0.004)
H $\delta$	4100	0.18	0.261 (0.005)	0.264 (0.006)	0.251 (0.010)	0.263 (0.015)	0.263 (0.048)	0.265 (0.005)
H $\gamma$	4340	0.14	0.471 (0.008)	0.469 (0.008)	0.469 (0.015)	0.466 (0.022)	0.470 (0.058)	0.469 (0.007)
[O III]	4363	0.13	0.041 (0.002)	0.024 (0.002)	0.095 (0.006)	< 0.008	< 0.022	< 0.001 <sup>u</sup>
He I	4471	0.10	0.036 (0.002)	0.028 (0.002)	0.027 (0.003)	—	—	0.029 (0.002)
[Ar IV]	4713	0.04	0.005 (0.001)	—	—	—	—	—
H $\beta$	4861	0.00	1.000 (0.013)	1.000 (0.013)	1.000 (0.024)	1.000 (0.038)	1.000 (0.086)	1.000 (0.012)
He I	4922	−0.01	0.007 (0.001)	—	—	—	—	—
[O III]	4959	−0.02	1.819 (0.022)	1.177 (0.015)	1.570 (0.034)	0.948 (0.036)	0.345 <sup>c</sup>	1.067 (0.013)
[O III]	5007	−0.03	5.531 (0.052)	3.605 (0.037)	4.637 (0.081)	2.906 (0.079)	1.260 (0.109)	3.272 (0.032)
He I	5876	−0.23	0.113 (0.003)	0.098 (0.003)	0.085 (0.006)	—	—	0.103 (0.003)
[O I]	6300	−0.30	0.016 (0.002)	0.054 (0.002)	0.017 (0.003)	—	—	0.031 (0.002)

Table 2—Continued

Line	$\lambda(\text{\AA})$	$f(\lambda)$	VCC 1699	VCC 144	VCC 1313	VCC 562	VCC 2033	VCC 324
[S III]	6312	−0.30	0.016 (0.001)	0.012 (0.001)	—	—	—	—
[N II]	6548	−0.34	0.025 (0.001)	0.069 (0.003)	—	0.025 <sup>u</sup>	—	0.061 (0.002)
H $\alpha$	6563	−0.34	2.868 (0.031)	2.859 (0.030)	2.861 (0.051)	2.848 (0.080)	2.865 (0.190)	2.860 (0.030)
[N II]	6584	−0.34	0.079 (0.003)	0.205 (0.003)	0.031 (0.003)	0.146 <sup>c</sup> (0.012)	0.259 (0.039)	0.198 (0.004)
He I	6678	−0.35	0.033 (0.002)	0.030 (0.001)	0.023 (0.002)	—	—	0.029 (0.002)
[S II]	6717	−0.36	0.104 (0.002)	0.181 (0.004)	0.116 (0.005)	0.298 (0.017)	0.859 (0.072)	0.244 (0.005)
[S II]	6731	−0.36	0.077 (0.003)	0.211 (0.004)	0.085 (0.004)	0.196 (0.013)	0.320 (0.039)	0.184 (0.004)
He I	7065	−0.40	0.026 (0.001)	0.019 (0.002)	0.023 (0.003)	—	—	—
[Ar III]	7135	−0.41	0.105 (0.003)	—	0.046 (0.004)	0.007 <sup>u</sup>	—	0.078 (0.003)
P14	8598	−0.62	0.005 (0.001)	—	—	—	—	—
P13	8665	−0.63	0.005 <sup>u</sup>	—	—	—	—	—
P10	9014	−0.67	0.013 (0.002)	—	—	—	—	—
[S III]	9069	−0.68	0.157 (0.006)	0.101 (0.006)	—	—	—	—
P9	9229	−0.70	0.016 <sup>u</sup>	—	—	—	—	—
[S III]	9532	−0.75	0.550 <sup>u</sup>	0.300 (0.014)	—	—	—	—
P8	9546	−0.75	0.025 <sup>u</sup>	—	—	—	—	—
$C(\text{H}\beta)$			0.14	0.08	0.01	0.11	0.10	0.23
$F(\text{H}\beta)$			54.4	42.8	12.1	16.4	2.14	80.5
$EW(\text{H}\beta)$			81	50	72	59	8	59

<sup>u</sup>Uncertain value

<sup>c</sup>Cosmic ray

Table 2. Continued.

Line	$\lambda(\text{\AA})$	$f(\lambda)$	VCC 848 <sup>1a</sup>	b	c	VCC 848 <sup>2</sup>	VCC 1437	VCC 841	VCC 334
[O II]	3727	0.26	1.989 (0.074)	2.968 (0.460)	2.573 (0.276)	3.410 (0.111)	4.816 (0.187)	2.714 (0.133)	3.725 (0.123)
[Ne III]	3868	0.23	0.233 (0.034)	—	—	—	—	—	—
H8 + He I	3889	0.22	0.115 (0.031)	—	—	—	—	—	—
He $\epsilon$ +[Ne III]	3969	0.21	0.160 (0.032)	—	—	—	—	—	—
H $\delta$	4100	0.18	0.261 (0.034)	0.262 (0.157)	—	0.247 <sup>u</sup> (0.027)	0.263 (0.039)	0.264 (0.027)	0.181 (0.012)
H $\gamma$	4340	0.14	0.467 (0.032)	0.468 (0.173)	0.470 <sup>u</sup>	0.472 (0.025)	0.466 (0.036)	0.466 (0.038)	0.473 (0.025)
[O III]	4363	0.13	0.046 (0.015)	< 0.079	< 0.040	0.041 (0.014)	< 0.014	< 0.014	< 0.018
H $\beta$	4861	0.00	1.000 (0.044)	1.000 (0.240)	1.000 (0.124)	1.000 (0.038)	1.000 (0.060)	1.000 (0.062)	1.000 (0.040)
[O III]	4959	−0.02	1.158 (0.049)	0.416 (0.168)	0.580 (0.094)	1.072 (0.041)	0.791 (0.053)	0.722 (0.051)	0.596 <sup>u</sup>
[O III]	5007	−0.03	3.526 (0.113)	1.524 (0.307)	1.180 (0.138)	3.211 (0.093)	2.482 (0.115)	2.448 (0.126)	2.005 (0.066)
He I	5876	−0.23	0.060 (0.012)	—	—	0.104 (0.018)	0.095 (0.016)	0.084 (0.016)	—
[O I]	6300	−0.30	0.030 (0.009)	—	—	0.082 (0.017)	—	0.024 (0.008)	—
[N II]	6548	−0.34	0.091 <sup>u</sup>	0.111 (0.045)	—	0.085 <sup>u</sup> (0.014)	0.145 (0.018)	0.102 <sup>u</sup>	0.040 <sup>u</sup>
H $\alpha$	6563	−0.34	2.853 (0.090)	2.853 (0.430)	2.864 (0.243)	2.849 (0.098)	2.851 (0.152)	2.850 (0.158)	2.873 (0.090)
[N II]	6584	−0.34	0.177 (0.012)	0.369 (0.082)	0.373 (0.061)	0.196 (0.018)	0.515 (0.038)	0.370 (0.034)	0.223 (0.019)
He I	6678	−0.35	—	—	—	—	—	0.017 (0.006)	—
[S II]	6717	−0.36	0.136 (0.012)	0.591 (0.114)	0.899 (0.100)	0.361 (0.022)	0.361 (0.031)	0.401 (0.035)	0.504 (0.026)
[S II]	6731	−0.36	0.107 (0.011)	0.448 (0.094)	0.474 (0.069)	0.253 (0.018)	0.276 (0.026)	0.280 (0.028)	0.358 (0.020)
[Ar III]	7135	−0.41	—	—	—	0.085 (0.013)	0.074 (0.013)	0.088 (0.013)	—

Table 2—Continued

Line	$\lambda(\text{\AA})$	$f(\lambda)$	VCC 848 <sup>1a</sup>	b	c	VCC 848 <sup>2</sup>	VCC 1437	VCC 841	VCC 334
$C(\text{H}\beta)$			0.07	0.12	0.06	0.22	0.43	0.40	0.13
$F(\text{H}\beta)$			6.71	2.11	1.55	14.2	12.4	7.76	8.31
$EW(\text{H}\beta)$			32	5	14	14	5	21	13

<sup>a</sup>Uncertain value

<sup>1</sup>Spectra of knots a, b and c (figure 1); 1993 run

<sup>2</sup>Integrated spectrum; 1994 run

Table 2. Continued.

Line	$\lambda(\text{\AA})$	$f(\lambda)$	VCC 1374	VCC 655	VCC 1725	VCC 135	VCC 1486	VCC 1955
[O II]	3727	0.26	3.007 (0.065)	2.035 (0.140)	2.959 (0.129)	1.344 (0.113)	3.763 (0.264)	1.973 (0.064)
H $\delta$	4100	0.18	0.266 (0.014)	0.266 (0.044)	0.261 <sup>u</sup> (0.022)	0.263 <sup>u</sup> (0.060)	0.263 <sup>u</sup> (0.055)	0.261 <sup>u</sup> (0.020)
H $\gamma$	4340	0.14	0.470 (0.017)	—	0.469 (0.029)	0.469 (0.051)	0.470 (0.061)	0.469 (0.022)
[O III]	4363	0.13	0.015 (0.006)	< 0.041	0.035 (0.012)	< 0.032	< 0.030	< 0.010
H $\beta$	4861	0.00	1.000 (0.026)	1.000 (0.075)	1.000 (0.046)	1.000 (0.073)	1.000 (0.103)	1.000 (0.036)
[O III]	4959	−0.02	1.036 (0.027)	—	0.647 (0.037)	0.109:	—	0.105 (0.014)
[O III]	5007	−0.03	2.995 (0.059)	0.186 (0.039)	1.853 (0.070)	0.226 (0.048)	0.814 (0.095)	0.290 (0.019)
He I	5876	−0.23	0.111 (0.012)	—	—	—	—	0.084 (0.018)
[O I]	6300	−0.30	—	—	—	—	—	0.065 (0.013)
[N II]	6548	−0.34	0.077 (0.009)	0.226 <sup>u</sup> (0.040)	0.157 <sup>u</sup> (0.023)	0.258 (0.074)	0.238 (0.060)	0.208 (0.019)
H $\alpha$	6563	−0.34	2.880 (0.065)	2.871 (0.203)	2.867 (0.099)	2.866 (0.211)	2.869 (0.264)	2.866 (0.102)
[N II]	6584	−0.34	0.242 (0.013)	0.821 (0.078)	0.386 (0.030)	0.907 (0.084)	0.595 (0.089)	0.647 (0.034)
[S II]	6717	−0.36	0.413 (0.017)	0.548 (0.060)	0.572 (0.032)	0.466 (0.073)	0.690 (0.099)	0.468 (0.027)
[S II]	6731	−0.36	0.294 (0.015)	0.404 (0.051)	0.403 (0.027)	0.321 (0.063)	0.561 (0.091)	0.334 (0.022)
[Ar III]	7135	−0.41	0.087 (0.012)	0.068 (0.026)	0.117 (0.017)	—	—	0.046 (0.012)
$C(\text{H}\beta)$			0.22	0.44	0.04	0.52	0.36	0.39
$F(\text{H}\beta)$			23.2	9.17	7.34	5.85	3.67	14.8
$EW(\text{H}\beta)$			16	4	18	4	5	12

<sup>u</sup>Uncertain value

Table 2. Continued.

Line	$\lambda(\text{\AA})$	$f(\lambda)$	VCC 2037	VCC 72	VCC 428	VCC 802	VCC 213	VCC 1179
[O II]	3727	0.26	5.438 (0.488)	3.424 (0.408)	2.128 (0.070)	2.696 (0.160)	2.361 (0.121)	9.503 (1.124)
[Ne III]	3868	0.23	—	—	0.214 (0.023)	0.303 (0.053)	—	—
H8 + He I	3889	0.22	—	—	0.150 (0.022)	0.203 (0.048)	—	—
He $\epsilon$ + [Ne III]	3969	0.21	—	—	0.188 (0.022)	—	—	—
H $\delta$	4100	0.18	—	0.261 <sup>u</sup> (0.109)	0.262 (0.017)	0.259 <sup>u</sup> (0.036)	0.261 (0.044)	0.262 (0.116)
H $\gamma$	4340	0.14	0.469 (0.095)	0.467 (0.126)	0.470 (0.022)	0.468 (0.041)	—	0.469 <sup>u</sup> (0.126)
[O III]	4363	0.13	< 0.047	< 0.063	0.072 (0.012)	0.031 (0.013)	< 0.028	< 0.055
H $\beta$	4861	0.00	1.000 (0.128)	1.000 (0.149)	1.000 (0.031)	1.000 (0.068)	1.000 (0.065)	1.000 (0.169)
[O III]	4959	−0.02	0.682 (0.111)	—	0.963 (0.031)	0.700 (0.055)	0.109 (0.043)	0.471 (0.119)
[O III]	5007	−0.03	1.812 (0.200)	0.477 (0.105)	2.910 (0.072)	2.150 (0.121)	0.336 (0.051)	1.525 (0.223)
He I	5876	−0.23	—	—	—	—	0.219 (0.043)	—
[O I]	6300	−0.30	—	—	—	—	—	—
[N II]	6548	−0.34	—	0.315 <sup>u</sup> (0.131)	—	0.103 (0.031)	0.259 (0.039)	0.216 <sup>u</sup> (0.096)
H $\alpha$	6563	−0.34	2.863 (0.345)	2.861 (0.363)	2.871 (0.083)	2.858 (0.179)	2.858 (0.180)	2.864 (0.363)
[N II]	6584	−0.34	0.354 (0.109)	0.729 (0.170)	0.072 (0.012)	0.355 (0.046)	0.910 (0.076)	0.434 (0.117)
[S II]	6717	−0.36	0.781 (0.129)	1.525 <sup>u</sup> (0.243)	0.173 (0.015)	0.481 (0.053)	0.473 (0.052)	0.710 (0.146)
[S II]	6731	−0.36	0.630 (0.113)	0.445 (0.143)	0.135 (0.014)	0.355 (0.046)	0.364 (0.046)	0.559 (0.130)
He I	7065	−0.40	—	—	0.037 (0.009)	—	—	—
[Ar III]	7135	−0.41	—	—	0.061 (0.010)	—	—	0.209 (0.099)

Table 2—Continued

Line	$\lambda(\text{\AA})$	$f(\lambda)$	VCC 2037	VCC 72	VCC 428	VCC 802	VCC 213	VCC 1179
$C(\text{H}\beta)$			0.30	0.10	0.23	0.25	0.48	0.04
$F(\text{H}\beta)$			1.54	0.755	12.5	3.13	14.3	0.655
$EW(\text{H}\beta)$			6	—	63	21	5	2

<sup>u</sup>Uncertain value

Table 3. Comparison of values of  $\log R_{23}$  with previous works. (1) Galaxy VCC number; (2) IG89: Izotov and Guseva (1989); (3) GH89: Gallagher and Hunter (1989); (4) this work.

VCC	IG89	GH89	this work
144	0.86	0.89	0.865
324	0.72	0.88	0.817
334	–	0.91	0.80
848	–	0.73 <sup>u</sup>	0.824
1374	–	0.92 <sup>u</sup>	0.85
1437	0.74	–	0.908
1725	–	0.81	0.74
2033	0.89	0.91	0.665

<sup>u</sup>uncertain value



Table 4. Direct determination of physical conditions and abundances

	VCC 1699	VCC 144	VCC 1313	VCC 848 <sup>a</sup>	VCC 848 <sup>i</sup>	VCC 1374	VCC 1725	VCC 428	VCC 802
Te <sub>[OIII]</sub> (10 <sup>4</sup> K)	1.048±0.021	1.014±0.037	1.542±0.038	1.278±0.132	1.265±0.131	0.929±0.090	1.481±0.150	1.696±0.10	1.33±0.14
Te <sub>[SIII]</sub> (10 <sup>4</sup> K)	1.06±0.03	1.15±0.03	–	–	–	–	–	–	–
log Ne <sub>[SII]</sub> (cm <sup>-3</sup> )	1.9	1.8	1.8	2.2	≤2	≤2	≤2	2.1	1.8
12 + log (O <sup>+</sup> /H <sup>+</sup> )	7.61±0.05	8.00±0.07	7.08±0.07	7.57±0.15	7.72±0.16	7.94±0.16	7.54±0.15	7.30±0.10	7.58±0.16
12 + log (O <sup>++</sup> /H <sup>+</sup> )	8.23±0.06	8.09±0.05	7.67±0.05	7.76±0.12	7.74±0.16	8.14±0.10	7.31±0.11	7.36±0.08	7.50±0.14
12 + log (O/H)	8.32±0.06	8.35±0.07	7.77±0.06	7.98±0.14	8.03±0.16	8.35±0.14	7.74±0.14	7.64±0.09	7.84±0.15
log (N <sup>+</sup> /O <sup>+</sup> )	-1.46±0.05	-1.39±0.04	-1.63±0.08	-1.22±0.08	-1.37±0.11	-1.33±0.09	-0.97±0.10	-1.53±0.10	-1.0±0.12
12 + log (S <sup>+</sup> /H <sup>+</sup> )	5.58±0.05	6.04±0.04	5.36±0.06	5.58±0.14	5.90±0.16	6.31±0.12	6.00±0.11	5.39±0.11	6.02±0.17
12 + log (S <sup>++</sup> /H <sup>+</sup> )	6.57±0.08	6.40±0.09	–	–	–	–	–	–	–
12 + log (S/H)	≥6.61±0.08	≥6.56±0.08	–	–	–	–	–	–	–
log (Ne <sup>++</sup> /O <sup>++</sup> )	-0.70±0.03	-0.64±0.06	-0.74±0.07	-0.74±0.08	–	–	–	-0.74±0.10	-0.46±0.17
log (Ar <sup>++</sup> /O <sup>++</sup> )	-2.29±0.08	–	-2.42±0.09	–	-2.06±0.09	-2.16±0.10	-1.62±0.12	-2.06±0.10	–

<sup>a</sup>Knot a, 1993 run

<sup>i</sup>Integrated spectrum, 1994 run

Table 5. Adopted abundances and ionization structure parameters for Virgo dwarf galaxies.

VCC	1699	144	1313	562	2033	324	848	1437	841	334
log R <sub>23</sub>	0.935	0.865	0.864	0.814	0.665	0.817	0.824	0.908	0.770	0.80
log ([OIII]/[OII])	0.688	0.275	0.751	0.162	-0.274	0.292	0.372	-0.168	0.067	-0.156
log ([NII]/[OII])	-1.10	-0.96	-1.40	-1.15 <sup>u</sup>	-0.96 <sup>a</sup>	-0.92	-0.92	-0.85	-0.77	-1.15
12 + log (O/H)										
[OIII] $\lambda$ 4363 <sup>1</sup>	8.32	8.35	7.77	$\geq 8.5$	$\geq 7.7$	–	7.98 (8.03) <sup>i</sup>	$\geq 8.5$	$\geq 8.31$	$\geq 8.1$
P <sub>upper</sub> <sup>2</sup>	8.38	8.35	8.49	8.38	8.40	8.42	8.44 (8.25) <sup>i</sup>	8.10	8.40	8.27
P <sub>lower</sub> <sup>2</sup>	7.85	7.93	7.73	7.93	8.11	7.85	7.81 (8.05) <sup>i</sup>	8.05	7.93	8.18
R <sub>23upper</sub> <sup>3</sup>	8.52	8.54	8.61	8.58	8.71	8.60	8.60 (8.5) <sup>i</sup>	8.41	8.63	8.56
R <sub>23lower</sub> <sup>3</sup>	8.09	8.08	7.92	8.02	7.93	7.99	7.97 (7.9) <sup>i</sup>	8.30	7.98	8.11
[NII]/[OII] <sup>4</sup>	8.5	8.5	7.9 <sup>u</sup>	8.5	8.6	8.6	8.5	8.6	8.7	8.5
S <sub>23</sub> <sup>5</sup>	8.20	8.10	–	–	–	–	–	–	–	–
Adopted										
<12 + log (O/H)>	8.32	8.35	7.77	8.6-8.4 <sup>a</sup>	8.7-8.4 <sup>a</sup>	8.6-8.4	8.0	8.3 $\pm$ 0.2	8.7-8.4	8.2-8.1
<log (N/O)>	-1.46	-1.39	-1.63	-1.6 <sup>a</sup>	-1.5 <sup>a</sup>	-1.4	-1.30	-1.3	-1.3	-1.4

<sup>u</sup>Uncertain value

<sup>i</sup>Abundances derived from the integrated spectrum of A1223+06 (in parenthesis)

<sup>a</sup>At the 1 $\sigma$  error level, [NII]/[OII]  $\leq$  0.1 could be compatible, leading to <12 + log (O/H)> = 8.0 , <log (N/O)> = -1.4

<sup>1</sup>Direct abundance determination (or lower limit) from the [OIII]  $\lambda$ 4363 line flux

<sup>2</sup>P-method calibration, upper-lower branch after Pilyugin (2000; 2001)

<sup>3</sup>Calibration of R<sub>23</sub> (cf. Pagel et al. 1980), according to the theoretical models of McGaugh (1991): upper-lower branch as parameterized in Kobulnicky et al. (1999)

<sup>4</sup>Calibration of the [NII]/[OII] abundance diagnostic according to the theoretical models of Dopita et al. (2000)

<sup>5</sup>Empirical calibration using sulphur lines, after Díaz and Pérez-Montero (2000)

Table 5. Continued.

VCC	1374	655	1725	135	1486	1955	2037	428	802	213	1179
$\log R_{23}$	0.85	0.36	0.74	0.22	0.69	0.37	0.90	0.78	0.74	0.45	1.06
$\text{Log} ([\text{OIII}]/[\text{OII}])$	0.13	-0.93	-0.07	-0.64	-0.54	-0.70	-0.34	0.26	0.02	-0.73	-0.68
$\log ([\text{NII}]/[\text{OII}])$	-0.98	-0.28	-0.77	-0.06	-0.69	-0.37	-1.07	-1.35	-0.77	-0.30	-1.22
$12 + \log (\text{O}/\text{H})$											
$[\text{OIII}] \lambda 4363$ <sup>1</sup>	8.35	–	7.74	–	$\geq 7.3$	–	$\geq 7.7$	7.64	7.84	–	$\geq 7.7$
$P_{upper}$ <sup>2</sup>	8.3	8.6	8.4	8.7	8.3	8.6	8.1	8.5	8.4	8.5	<sup>u</sup>
$P_{lower}$ <sup>2</sup>	8.0	8.5	8.0	7.9	8.4	8.2	8.5	7.8	7.9	8.4	<sup>u</sup>
$R_{23upper}$ <sup>3</sup>	8.5	8.9	8.6	8.9	8.6	8.9	8.4	8.6	8.6	8.9	8.2
$R_{23lower}$ <sup>3</sup>	8.1	7.75	8.0	7.5	8.1	7.7	8.3	7.9	7.9	7.8	8.2
$[\text{NII}]/[\text{OII}]$ <sup>4</sup>	8.6	8.8	8.7	8.9	8.7	8.9	8.4	8.1	8.7	8.9	8.0
Adopted											
$\langle 12 + \log (\text{O}/\text{H}) \rangle$	8.35	8.9-8.6	7.74	8.9-8.7	8.7-8.3	8.9-8.6	$8.3 \pm 0.2$	7.64	7.84	8.9-8.5	$8.2 \pm 0.2$
$\langle \log (\text{N}/\text{O}) \rangle$	-1.33	-0.9	-0.97	-0.75	-1.2	-1.0	-1.5	-1.53	-1.0	-0.9	-1.5

<sup>u</sup>Uncertain value or calibration

<sup>1</sup>Direct abundance determination (or lower limit) from the  $[\text{OIII}] \lambda 4363$  line flux

<sup>2</sup>P-method calibration, upper-lower branch after Pilyugin (2000; 2001)

<sup>3</sup>Calibration of  $R_{23}$  (cf. Pagel et al. 1980), according to the theoretical models of McGaugh (1991): upper-lower branch as parameterized in Kobulnicky et al. (1999)

<sup>4</sup>Calibration of the  $[\text{NII}]/[\text{OII}]$  abundance diagnostic according to the theoretical models of Dopita et al. (2000)

<sup>5</sup>Empirical calibration using sulphur lines, after Díaz and Pérez-Montero (2000)